Journal of Medicinal Chemistry

pubs.acs.org/jmc Article

Imidazopyridine-Based 5-HT$_6$ Receptor Neutral Antagonists: Impact of N^1-Benzyl and N^1-Phenylsulfonyl Fragments on Different Receptor Conformational States

David Vanda, Vittorio Canale, Severine Chaumont-Dubel, Rafał Kurczab, Grzegorz Satała, Paulina Koczurkiewicz-Adamczyk, Martyna Krawczyk, Wojciech Pietruś, Klaudia Blicharz, Elżbieta Pękala, Andrzej J. Bojarski, Piotr Popik, Philippe Marin, Miroslav Soural,* and Paweł Zajdel*

Cite This: *J. Med. Chem.* 2021, 64, 1180−1196 Read Online

ACCESS | Metrics & More | Article Recommendations | Supporting Information

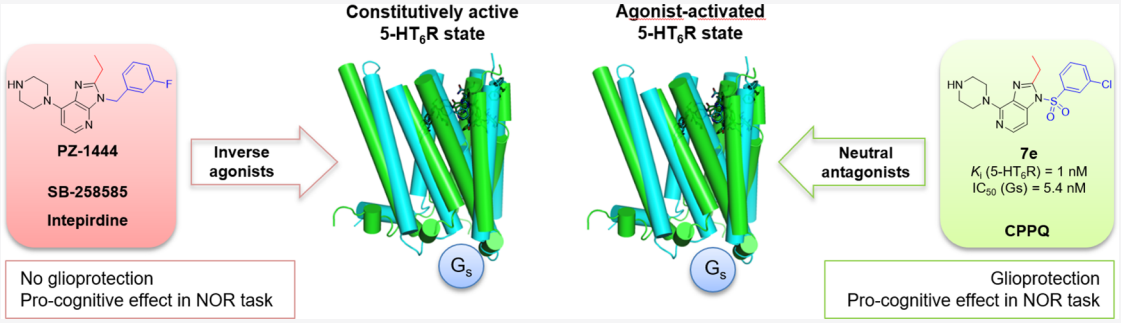

ABSTRACT: G-protein coupled receptors (GPCRs) exist in an equilibrium of multiple conformational states, including different active states, which depend on the nature of the bound ligand. In consequence, different conformational states can initiate specific signal transduction pathways. The study identified compound **7e**, which acts as a potent 5-hydroxytryptamine type 6 receptor (5-HT$_6$R) neutral antagonist at Gs and does not impact neurite growth (process controlled by Cdk5). MD simulations highlighted receptor conformational changes for **7e** and inverse agonist PZ-1444. In cell-based assays, neutral antagonists of the 5-HT$_6$R (**7e** and CPPQ), but not inverse agonists (SB-258585, intepirdine, PZ-1444), displayed glioprotective properties against 6-hydroxydopamine-induced and doxorubicin-induced cytotoxicity. These suggest that targeting the activated conformational state of the 5-HT$_6$R with neutral antagonists implicates the protecting properties of astrocytes. Additionally, **7e** prevented scopolamine-induced learning deficits in the novel object recognition test in rats. We propose **7e** as a probe for further understanding of the functional outcomes of different states of the 5-HT$_6$R.

INTRODUCTION

The 5-hydroxytryptamine type 6 receptor (5-HT$_6$R) is a Gs-coupled receptor[1] that raises increasing interest as a target for treatment of the cognitive impairments of neurodegenerative and psychiatric disorders.[2−4] In addition to the canonical Gs-adenylyl cyclase signaling pathway, the 5-HT$_6$R engages mechanistic target of rapamycin (mTOR) and cyclin-dependent kinase 5 (Cdk5) signaling,[5] two pathways involved in brain development and synaptic plasticity.[6,7]

An important feature of the 5-HT$_6$R is its high level of ligand-independent constitutive activity. This ability of the 5-HT$_6$R to activate a second messenger in the absence of agonist was first established *in vitro* using recombinant receptors expressed in a cell line[8] and subsequently confirmed in primary cultured neurons containing native receptors as well as in the brain of mice.[9] Considering that receptor constitutive activity as well as agonist-induced receptor activation might be involved in pathophysiological mechanisms, the design of 5-HT$_6$R ligands displaying inverse agonist or neutral antagonist properties may allow the systematic exploration of distinct pharmacological responses associated with a particular functional profile.

The beneficial effects of 5-HT$_6$R antagonists on cognition have been demonstrated in various paradigms of cognitive impairments.[10−14] They have been attributed to the predominant localization of the 5-HT$_6$R in brain regions implicated in mnemonic and cognitive functions, where the blockade of receptors located on GABAergic interneurons increases glutamatergic and cholinergic transmission through the relief

Received: November 19, 2020
Published: January 13, 2021

https://dx.doi.org/10.1021/acs.jmedchem.0c02009
J. Med. Chem. 2021, 64, 1180−1196

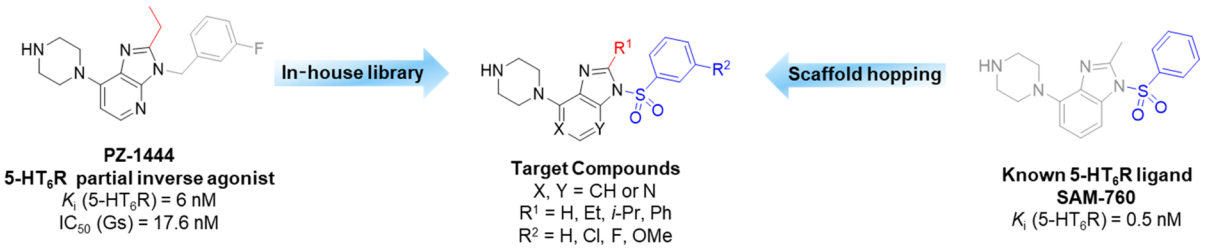

Figure 1. Rational design toward the *N*-phenylsulfonyl-imidazopyridine focused library.

Scheme 1. Synthetic Pathway Leading to *N*-Phenylsulfonyl-imidazo[4,5-*c*]pyridines[a]

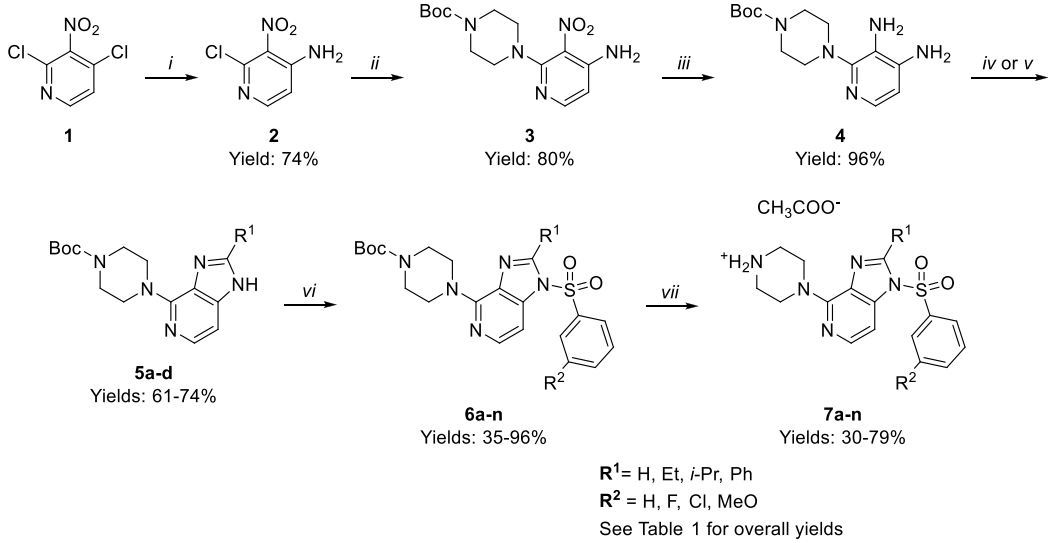

[a]Reagents and conditions: (i) NH_3 (aq, 25%), dimethyl sulfoxide (DMSO), 80 °C, 2 h; (ii) *N*-Boc-piperazine, *N*,*N*-diisopropylethylamine (DIEA), DMSO, 80 °C, 2−3 h; (iii) H_2, 10% Pd/C, EtOH, rt, 16 h; (iv) (for R^1 = H) triethyl orthoformate, DMSO, 100 °C, 1 h; (v) (for R^1 = Et, *i*-Pr, Ph) aldehyde, *N*,*N*-dimethylformamide (DMF), 90 °C, 16 h; (vi) arylsulfonyl chloride, (*tert*-butylimino)tris(pyrrolidino)phosphorane (BTPP), dichloromethane (DCM), 0 °C → rt, 16 h; (vii) (1) 10% trifluoroacetic acid (TFA) in DCM, rt, 1−2 h; (2) Na_2CO_3 (neutralization), then AcOH, rt, 30 min.

of GABAergic inhibition.[15,16] Of note, studies have also shown pro-cognitive effects of 5-HT_6R agonists,[17,18] which might reflect their ability to activate the Gs-adenylyl cyclase pathway, thus promoting cAMP formation, whereas pro-cognitive effects of antagonists were attributed to the blockade of 5-HT_6 receptor-operated mTORC1 signaling.[5,19,20]

Despite encouraging preclinical studies, the recent failure of two 5-HT_6R antagonists (intepirdine and idalopirdine) in phase III clinical trials for Alzheimer's disease calls for a more detailed exploration of the cellular and neurochemical mechanisms underlying the control of cognitive processes by the 5-HT_6R.[21] Another level of complexity might arise from the non-selective profile of the compounds previously evaluated in phase III clinical studies, underscoring the need to develop new 5-HT_6R ligands with better selectivity, with distinct pharmacological effects on the receptor (inverse agonists *vs.* neutral antagonists) and those that affect specific receptor-operated pathways.[22]

In this study, we employed a bioisosteric replacement in imidazopyridine-based 5-HT_6R ligands[23] to explore the impact of N^1-benzyl and N^1-phenylsulfonyl fragments on the active and inactive states of the receptor. The study originated from a recent report on N^1-benzylimidazo[4,5-*b*]pyridines and imidazo[4,5-*c*]pyridines,[24] which identified compound PZ-1444 (2-ethyl-3-(3-fluorobenzyl)-7-(piperazin-1-yl)-3*H*-imidazo[4,5-*b*]pyridine), a 5-HT_6R partial inverse agonist at Gs (Figure 1).

Regarding the high preference for the sulfone/sulfonamide moiety to generate potent 5-HT_6R ligands, we undertook the structural optimization of imidazo[4,5-*b*]pyridines and imidazo[4,5-*c*]pyridines, by replacing the N^1-benzyl group of compound PZ-1444 with an N^1-phenylsulfonyl fragment, to evaluate the impact of an additional H-bond acceptor group on the binding at the 5-HT_6R. Since the quest for indole-derived 5-HT_6R ligands involved development of azaindole and benzimidazole analogues,[25,26] this study also examined a scaffold-hopping approach that originated from studying the impact of introducing a nitrogen atom to benzimidazole ring (an additional H-bond donor group) on the interaction with 5-HT_6R. Considering that N^1-benzyl and N^1-phenylsulfonyl imidazopyridines likely bind to the receptor in a different manner, the present work was also designed to specifically examine the interaction of the ligands with 5-HT_6R using molecular dynamics simulations. We found specific amino acid residues in the receptor binding pocket, which might account for the compound's modulation of receptor-operated Gs signaling. Since astrocytes are involved in the pathophysiology of neurodegenerative diseases by modulating oxidative stress and neuroinflammation, we wondered whether 5-HT_6R antagonists could prevent glial death and evaluated the ability of selected 5-HT_6R inverse agonists and neutral antagonists to

https://dx.doi.org/10.1021/acs.jmedchem.0c02009
J. Med. Chem. 2021, 64, 1180−1196

protect astrocytes against doxorubicin (DOX)-induced and 6-hydroxydopamine (6-OHDA)-induced toxicity. Finally, we examined whether compound **7e**, the selected 5-HT$_6$R neutral antagonist, may prevent scopolamine-induced cognitive decline in the novel object recognition (NOR) test in rats.

RESULTS AND DISCUSSION

Chemistry. The synthetic approach used for the preparation of N^1-phenylsulfonyl-imidazo[4,5-*c*]pyridines is depicted in Scheme 1. Reaction of readily available 2,4-dichloro-3-nitropyridine **1** with ammonia yielded compound **2**, which was subjected to substitution with *N*-Boc-piperazine to obtain intermediate **3**. Compound **3** was then reduced to amino derivative **4** using catalytic hydrogenation. Subsequent cyclization to imidazopyridines **5** was performed with triethyl orthoformate and different aldehydes, depending on the desired substitution at the C^2 position. Imidazopyridines **5a−d** were reacted with selected benzenesulfonyl chlorides using (*tert*-butylimino)tris(pyrrolidino)phosphorane (BTPP) as a base, giving compounds **6a−n**. We kept in mind the possible N^1/N^3 sulfonylation as reported in the literature on the series of 5,6-disubstituted imidazopyridines;[27] however, after sulfonylation of compounds **5a−d**, we detected only a single product in crude reaction mixtures. Consequently, the presence of the sterically demanding Boc-piperazine moiety in position 4 directed sulfonylation exclusively to the N^1 position, similar to reported alkylation of 4-substituted benzimidazoles.[28] Final removal of the Boc group was initially performed using an alcoholic solution of hydrogen chloride to provide us with the corresponding products **7a−n** as hydrochlorides. Unexpectedly, an easy cleavage of the protecting group was accompanied with removal of the phenylsulfonyl moiety. Consequently, Boc-deprotected analogues of compounds **5a−d** were obtained as the main products. For this reason, compounds **6a−n** were submitted to Boc removal using 10% trifluoroacetic acid in dichloromethane, and after neutralization, they were treated with acetic acid to yield the final products **7a−n** as acetate salts. These salts are pharmacologically more preferable than trifluoroacetates (Table 1).

We also attempted to synthesize imidazo[4,5-*b*]pyridine analogues by applying the developed protocols to 4-chloro-3-nitropyridin-2-amine **8** as the starting material (Scheme 2). Although crude product **12** was detected by UPLC-UV-MS (see Supporting Information, Figure 1-SI), it decomposed during silica gel chromatography purification. The same results were obtained using crystallization of the crude compound **12** from methanol. In every case, only desulfonylated intermediate **11** was isolated.

The general instability of *N*-benzenesulfonyl imidazopyridines under acidic conditions observed within the reaction sequence prompted us to explore the properties of products **7a−n** in more detail. The mechanistic degradation of the sulfonamide functionality was presumably based on the phenomenon observed with *β*-sulfams (Scheme 1-SI).[29] Such limited stability under an acidic environment might significantly limit the potential therapeutic application of the final compounds due to decomposition after *per os* administration. For this reason, we studied the target compounds from the imidazo[4,5-*c*]pyridine subset to determine their stability in aqueous hydrochloric acid at low pH. All tested compounds did not decompose at pH = 1 after a 1 h incubation. Furthermore, the exposure of selected compound **7j** to pH = 1 for prolonged time (24 h) confirmed its sufficient chemical stability under gastrointestinal environmental conditions. Surprisingly, instability of final compounds in deuterated dimethyl sulfoxide (DMSO) was observed when collecting NMR data, which was successfully bypassed by using deuterated methanol instead of DMSO. Consequently, DMSO was also excluded from biological screening protocols to obtain reliable results.

Table 1. Binding Data of Synthesized Compounds 7a−n and References I and II at 5-HT$_6$R

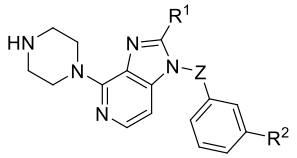

I; II; 7a-n

compd	Z	R^1	R^2	overall yield (%)	K_i [nM][a] 5-HT$_6$
I[b]	CH_2	H	H		450
II[b]	CH_2	H	Cl		320
7a	SO_2	H	H	22	3 ± 2
7b	SO_2	H	Cl	10	2 ± 1
7c	SO_2	H	F	22	3 ± 1
7d	SO_2	H	MeO	10	10 ± 2
7e	SO_2	Et	Cl	18	1 ± 0.5
7f	SO_2	Et	F	14	1 ± 0.3
7g	SO_2	*i*-Pr	H	16	2 ± 1
7h	SO_2	*i*-Pr	Cl	12	3 ± 2
7i	SO_2	*i*-Pr	F	18	1 ± 0.4
7j	SO_2	*i*-Pr	MeO	12	23 ± 4
7k	SO_2	Ph	H	9	119 ± 31
7l	SO_2	Ph	Cl	11	17 ± 3
7m	SO_2	Ph	F	13	37 ± 4
7n	SO_2	Ph	MeO	11	41 ± 9
intepirdine					1.4 ± 1

[a]Mean K_i values ± SEMs from three independent binding experiments. [b]Data taken from ref 24, where I and II encodes compounds **1** and **2**, respectively.

Structure−Activity Relationship Studies. While effectively optimizing molecular probes for a hypothesis-driven approach, we focused our attention on meeting the criteria of potency and drug-likeness properties. The prior reported series of arylsulfonamides of azaindole displayed high-to-moderate affinity for 5-HT$_6$R, though, for many of them, functional activity was not specified.[30,31] A strategy based on "flipping" arylsulfonyl group and amine moiety, applied by Bernotas *et al.*[32] revealed the preference of 4- and 7-azaindole core over 5- and 6-azaindoles. These studies hypothesized that the difference in basicity of the nitrogen in the pyridine ring might be responsible for higher activity of analogues with nitrogen close to bridge-headed carbons. A similar trend was observed for N^1-benzyl derivatives of imidazopyridines.[24] Localization of a nitrogen atom in the pyridine ring in distal position to the piperazine moiety (referring to 7-azaindole) was more favorable than when placed in proximal position to the piperazine moiety for the interaction of imidazo[4,5-*b*]pyridines with 5-HT$_6$R.

The results of the *in vitro* evaluation of imidazo[4,5-*c*]pyridines **7a−n** in [^{3}H]-LSD binding experiments for the 5-HT$_6$R (Table 1) showed that replacement of the N^1-benzyl fragment with the N^1-benzenesulfonyl moiety significantly

https://dx.doi.org/10.1021/acs.jmedchem.0c02009
J. Med. Chem. 2021, 64, 1180−1196

Scheme 2. Attempted Preparation of *N*-Phenylsulfonyl-imidazo[4,5-*b*]pyridines[a]

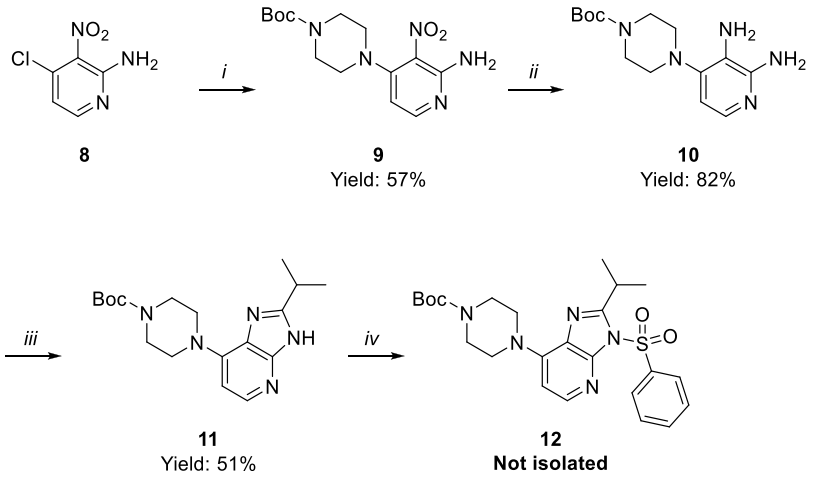

[a]Reagents and conditions: (i) *N*-Boc-piperazine, DIEA, DMSO, 80 °C, 3 h; (ii) H_2, 10% Pd/C, EtOH, rt, 16 h; (iii) isobutyraldehyde, DMSO, 90 °C, 16 h; (iv) benzenesulfonyl chloride, BTPP, DCM, 0 °C → rt, 16 h.

Table 2. Evaluation of Selected Compounds for Their Antagonist Property at 5-HT$_6$R in 1321N1 Cells, Their Functional Profile at 5-HT$_6$R-Dependent Gs Signaling in NG108-15 Cells, and Their Affinity for 5-HT$_{1A}$, 5-HT$_{2A}$, 5-HT$_6$, and D$_2$Rs

	5-HT$_6$				K_i [nM][a]			
compd	K_i [nM][a]	K_b [nM][b]	IC_{50} [nM][c]	functional profile[c]	5-HT$_{1A}$	5-HT$_{2A}$	5-HT$_7$	D$_2$
PZ-1444[d]	6 ± 3	3 ± 1	17.6 ± 1.98	inverse agonist	2790 ± 325	441 ± 87	12,340 ± 1204	3482 ± 267
7b	2 ± 1	59 ± 7	6.6 ± 1.2	neutral antagonist	285 ± 32	355 ± 64	6642 ± 1055	456 ± 85
7e	1 ± 0.5	35 ± 4	5.4 ± 1.4	neutral antagonist	146 ± 21	562 ± 72	3763 ± 350	886 ± 77
7f	1 ± 0.3	46 ± 12	6.4 ± 1.7	neutral antagonist	829 ± 99	264 ± 43	4300 ± 598	689 ± 91
7h	3 ± 2	31 ± 3	5.2 ± 1.9	neutral antagonist	307 ± 29	239 ± 28	3904 ± 374	1332 ± 146
7l	17 ± 3	258 ± 44	10.6 ± 2.7	neutral antagonist	1093 ± 104	410 ± 55	3084 ± 621	742 ± 80
intepirdine	1.4 ± 1	1 ± 0.4	2.8 ± 0.21	inverse agonist	2370 ± 367	26 ± 6	14,230 ± 1243	997 ± 124

[a]Mean K_i ± SEMs from three independent binding experiments. [b]Mean IC_{50} ± SEMs from three independent experiments in 1321N1 cells. [c]Mean IC_{50} ± SEMs from three independent experiments in NG108-15 cells. [d]Data taken from ref 24, where PZ-1444 is encoded as **17**.

improved the affinity of the compounds (**7a** *vs.* **II** and **7b** *vs.* **III**). To have a more in-depth analysis of ligand−receptor binding trends, we looked at the ligand lipophilicity efficiency (LLE) parameter. This parameter assesses the affinity of ligands for their receptors relative to their lipophilicity[33] and is often used to assess the quality of hit compounds. The LLE parameter has further confirmed the advantage of N^1-phenylsulfonyl derivatives.

The LLE was also used as a metric parameter to compare the properties of imidazopyridines *vs.* benzimidazole derivatives. Generally, an introduction of a nitrogen atom with H-bond donor properties to the benzimidazole core increases the hydrophilicity. An analysis revealed slightly higher LLE parameters for imidazo[4,5-*c*]pyridines **7a−n** over their benzimidazole analogues (analysis performed for pair of analogues for which biological data were available; Table 1-SI).

An analysis of pK_a, showed that the introduction of a nitrogen atom at the aromatic central scaffold in proximal position to the alicyclic amine moiety impacted compounds basicity. Indeed, pK_a values assessed using quantum calculations (Table 2-SI) revealed lower basicity of the piperazine moiety for imidazo[4,5-*c*]pyridine derivatives (pK_a ranged from 7.87 to 8.27), when compared to benzimidazole close analogues (pK_a = 8.41−9.24). In view of this finding, imidazo[4,5-*c*]pyridines **7a−n** might display low propensity to inhibit *h*ERG potassium channels and/or to induce phospholipidosis (drug-induced accumulation of phospholipidosis inside cells).[34]

Compounds bearing ethyl and isopropyl groups at the C^2 position of the imidazole moiety displayed high affinity for the 5-HT$_6$R (K_i < 25 nM) and showed similar potencies to the unsubstituted parent analogues (**7f** and **7i** *vs.* **7c**), confirming that small alkyl substituents were well tolerated. Although C^2-phenyl substituted *N*-benzenesulfonyl derivatives (**7k−n**) displayed the lowest potencies in the series, their affinity for the 5-HT$_6$R was still significantly higher compared with the *N*-benzyl analogues.[24]

Having previously identified the C^3 position on the N^1-benzyl fragment as the most privileged substitution pattern, the impact of selected substituents with different electronic properties was further investigated among the *N*-benzenesulfonyl analogues. Despite the ability of halogen atoms to stabilize the ligand−receptor complex *via* the formation of additional interactions (halogen bond, dipole−dipole, and van der Waals),[35−37] the introduction of 3-Cl and 3-F substituents at the phenylsulfonyl fragment did not significantly improve the affinity for the receptor compared to their unsubstituted analogues (**7a** *vs.* **7b** and **7c**, **7g** *vs.* **7h** and **7i**). However, among the C^2-substituted phenyl derivatives **7k−n**, this modification increased the affinity for the 5-HT$_6$R up to 7-fold (**7k** *vs.* **7l** and **7m**). Moreover, compounds with an electron-donating methoxy group showed less favorable interaction with the receptor, as demonstrated by the affinities

https://dx.doi.org/10.1021/acs.jmedchem.0c02009
J. Med. Chem. 2021, 64, 1180−1196

of compounds **7d**, **7j**, and **7n** (K_i = 10, 23, and 41 nM, respectively).

Impact of the Newly Generated 5-HT$_6$R Ligands on Receptor-Operated Signaling. In order to determine the structural determinants that might be responsible for their specificity toward different signaling pathways engaged by the 5-HT$_6$R, compounds with different C^2-substituents and N^1−3-chlorophenylsulfonyl fragment (**7b**, **7e**, **7h**, and **7l**) and compound **7f** (fluoro analogue of **7e**) were tested in a cAMP assay in 1321N1 cells expressing 5-HT$_6$R, with 5-CT as an agonist, to prove their antagonistic properties (Table 2). Then, selected compounds were further investigated for their ability to modulate 5-HT$_6$R-dependent Gs signaling in NG108-15 cells transiently expressing recombinant receptors, a cellular model that allows for the assessment of drug effects on 5-HT$_6$R constitutive activity in addition to agonist-stimulated activity.[6] All the evaluated compounds inhibited cAMP formation induced by treating cells with the 5-HT$_6$R agonist WAY181187 but did not affect the basal cAMP production elicited by 5-HT$_6$R expression. Compounds **7b**, **7e**, **7f**, **7h**, and **7l** were thus classified as neutral antagonists in this model (Table 2 and Figure 2), whereas intepirdine inhibited basal cAMP production in NG108-15 cells, indicative of inverse agonist effects.

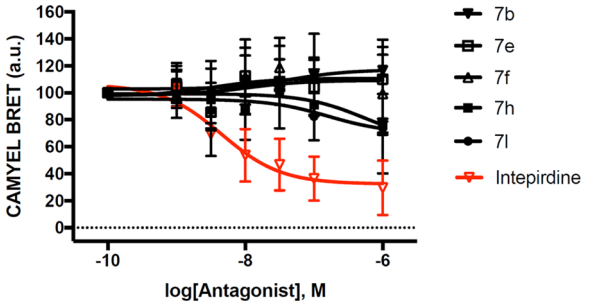

Figure 2. Evaluation of inverse agonist activity of compounds **7b**, **7e**, **7f**, **7h**, and **7l** on basal cAMP production in NG108-15 cells transiently transfected with plasmids encoding 5-HT$_6$R and the CAMYEL probe. 5-HT$_6$R antagonist intepirdine was used as a reference compound. For each compound, we performed three independent transfection experiments and measured data in quadruplicate. Data are given as means ± SEM of the values.

Although chemical instability of imidazo[4,5-*b*]pyridines derivatives (N^1-arylsulfonyl analogues of PZ-1444) did not allow for a direct comparison of close analogues bearing the same central imidazopyridine core, it seems that the type of N^1-substituent on the imidazole moiety might influence the functional profile of this group of derivatives, while the presence of the sulfonyl linker confers neutral antagonist properties, the more flexible N^1-benzyl fragment, present in PZ-1444, exhibits a different aromatic ring orientation that allows the inhibition of the 5-HT$_6$R constitutive activity at the Gs pathway. These findings might give additional insights into the rational design of novel 5-HT$_6$R modulators with different pharmacological profiles.

Selectivity Profile of Compounds 7b, 7e, 7f, 7h, and 7l. Selected compounds **7b**, **7e**, **7f**, **7h**, and **7l** were also profiled for their activity at serotonin 5-HT$_{1A}$, 5-HT$_{2A}$, 5-HT$_7$, and dopaminergic D$_2$ receptors (Table 2). Interaction with these receptors may impact body temperature (5-HT$_{1A}$ and 5-HT$_7$Rs), cause hallucinations (5-HT$_{2A}$R), or produce parkinsonian-like effect (D$_2$R). In line with the data for the N^1-benzyl-imidazo[4,5-*b*]pyridine derivatives,[24] the tested compounds displayed low affinity for 5-HT$_{2A}$ receptors (K_i > 260 nM) and high selectivity for 5-HT$_6$R over 5-HT$_7$ and D$_2$ receptors (up to 100-fold). Among the derivatives bearing an ethyl substituent in the C^2 position, compound **7e** showed higher affinity for 5-HT$_{1A}$R (K_i = 140 nM) than its 3-F analog **7f** (K_i = 829 nM), suggesting a potential role of a chlorine atom in the N^1-phenylsulfonyl fragment for interaction with the 5-HT$_{1A}$R subtype. Further functional profiling of **7e** at 5-HT$_{1A}$R showed low agonist activity (measurement of cAMP production in HEK293 cells; EC$_{50}$ > 2 μM) and no antagonist activity (measurement of the forskolin-induced cAMP production).

Preliminary *In itro* ADME/Tox Properties and Safety Evaluation. Early *in vitro* screening of metabolic stability represents an essential component in developing molecular probes as well as a key factor for the selection of lead compound for further preclinical development. Thus, compounds **7b**, **7e**, **7f**, **7h**, and **7l** were tested using *in vitro* assays to assess their metabolic stability in rat liver microsomes (RLM). Results showed that a fluorine atom was less favorable than chlorine at the N^1-phenylsulfonyl fragment (Cl$_{int}$ = 28.7 mL/min/kg for **7f**). Compound **7e** with an ethyl substituent in the C^2 position at the imidazole moiety displayed the lowest clearance value (Cl$_{int}$ = 24.1 mL/min/kg) when compared to unsubstituted and phenyl analogues (**7b**, Cl$_{int}$ = 38.3 mL/min/kg and **7l** Cl$_{int}$ = 55.7 mL/min/kg, respectively). In line with results from *in silico* assessment[38] (for more information, see Figure 3-SI), isopropyl derivative **7h** displayed the highest clearance value (79.4 mL/min/kg).

Compound **7e** was subsequently selected for *in vitro* screening of drug-like properties (Table 3). First, the aqueous solubility of compound **7e** at a physiologically relevant pH value of 7.4 was determined, revealing that it was readily soluble in water (168.5 mg/mL; 500 μmol/mL). The presence of a sulfonyl moiety together with the different condensations of the imidazopyridine core increased the solubility up to 10-fold compared to PZ-1444.

Considering that drug distribution into the brain is a prerequisite for CNS-acting compounds, the ability of compound **7e** to penetrate the BBB was evaluated in PAMPA assays. The results indicate that compound **7e** could be classified as highly brain penetrant under the tested conditions, exhibiting a permeability coefficient (Pe) value

Table 3. Preliminary ADME/Tox Profile for Compound 7e and PZ-1444

assay type	7e	PZ-1444
solubility (pH = 7.4)[a]	500 μmol/mL	50 μmol/mL
solubility (pH = 2.4)[b]	260 μmol/mL	25 μmol/mL
microsomal stability[c]	Cl$_{int}$ = 24.1 mL/min/kg	Cl$_{int}$ = 1.73 mL/min/kg
PAMPA permeability[d]	Pe = 6.97 × 10^{-6} cm/s	Pe = 5.84 × 10^{-6} cm/s
hepatotoxicity[e]	IC$_{50}$ > 50 μM	IC$_{50}$ > 50 μM
neurotoxicity[f]	IC$_{50}$ > 50 μM	IC$_{50}$ > 50 μM

[a]Measured in PBS. [b]Measured in acetate buffer. [c]Assessed in the RLM test, at a protein concentration of 0.2 mg/mL. [d]Measured at an initial concentration of 100 μM at pH 7.4. [e]IC$_{50}$ values were obtained upon treatment of HepG2 cells for 24 h; data from three independent experiments. [f]IC$_{50}$ values were obtained upon treatment of SH-SY5Y cells for 24 h; data from three independent experiments.

https://dx.doi.org/10.1021/acs.jmedchem.0c02009
J. Med. Chem. 2021, 64, 1180−1196

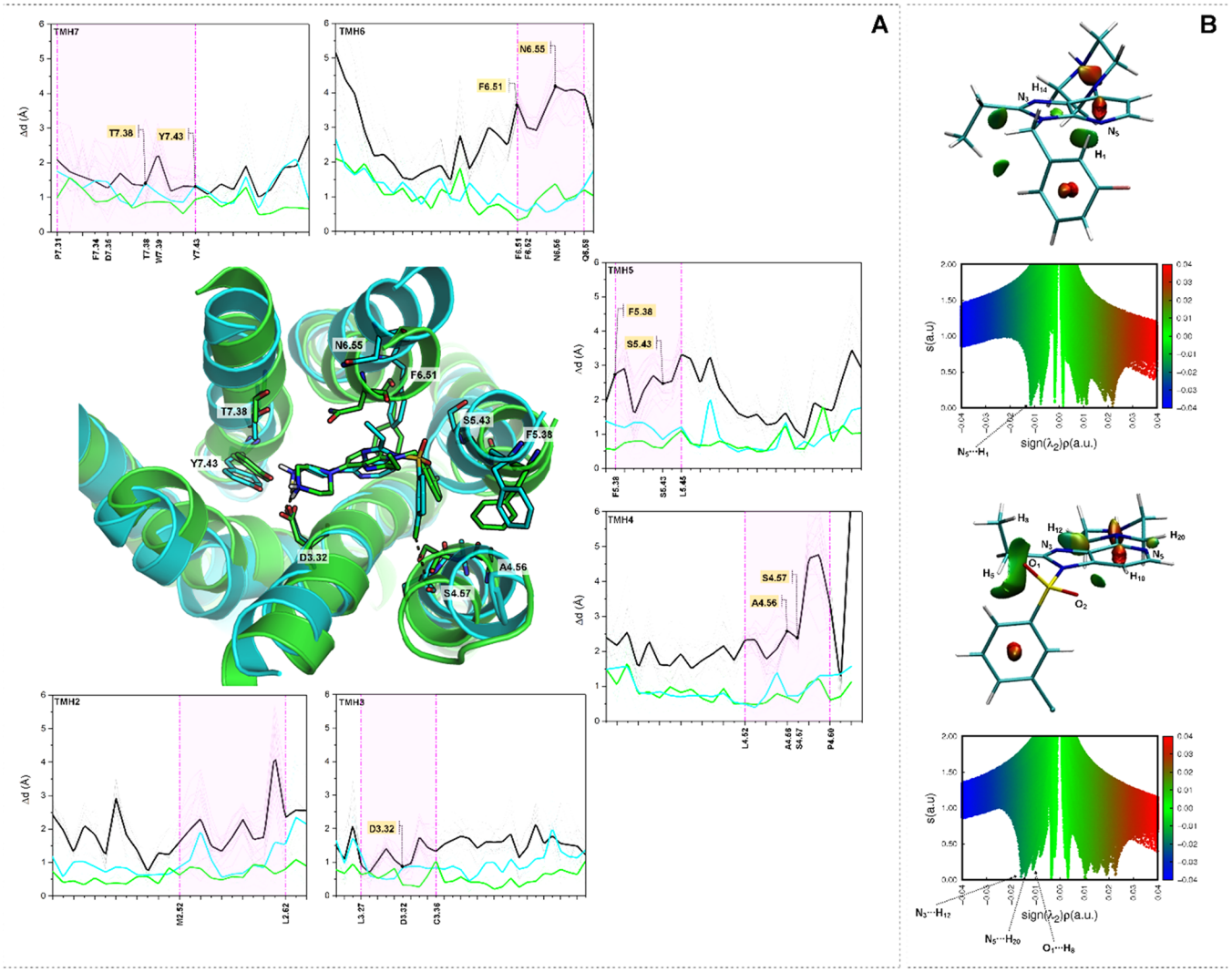

Figure 3. (A) Comparison of the binding mode of PZ-1444 (green) and compound **7e** (cyan) to the most populated conformation of 5-HT$_6$R obtained from the clustering of the MD trajectory. The homology model was built on a β_2 adrenergic template (PDB ID: 4LDE). For each helix, plots showing the relationship between the position of the geometric center of a given amino acid, calculated as the mean difference between conformations selected on the basis of MD trajectory clustering (green and blue line for the complexes of 5-HT$_6$R with PZ-1444 and compound **7e**, respectively), were drawn. The black line on these graphs displays the average differences in the position of a given amino acid between all pairs of conformations of PZ-1444 and compound **7e**. Additionally, fragments of the sequence of a given helix are marked by the pink area to determine the amino acids that form the binding site of the receptor. (B) Illustration of the intramolecular interactions via the gradient isosurfaces and the corresponding reduced density gradient (RDG) plots *vs.* the electron density multiplied by the sign of the second Hessian eigenvalue for the PZ-1444- and compound **7e**-elicited conformations isolated from the most populated MD cluster. Spikes located in the green to blue region indicate weak attractive interactions ($\lambda_2 < 0$), whereas those in green to red indicate repulsive interactions ($\lambda_2 > 0$). The egg-shaped fields refer to delocalized electrons of aromatic rings and were visualized for gradient surface factor $s = 0.1$ a.u.

comparable to that of the inverse agonist PZ-1444. Verapamil, a drug with high brain penetration (Pe = 1.85 × 10^{-5} cm/s), and doxorubicin with low brain penetration (no detection in the acceptor compartment) were used as reference compounds.

Additionally, preliminary hepatotoxicity and neurotoxicity risk assessment was implemented for compound **7e** using a human liver cancer cell line (HepG2) and a human neuroblastoma cell (SH-SY5Y). Compound **7e** did not impact both cell lines viability after a period of 24 h in the MTT assay (Table 3). A cytotoxic drug doxorubicin revealed more than 20-fold higher cytotoxic effect (IC_{50} = 2.3 μM).

Finally, compound **7e** displayed low affinity for α_{1A} adrenergic receptor (% inh. at 1 μM = 22%), β_1 adrenoreceptor (% inh. at 1 μM = 10%), *h*ERG channel (% inh. at 1 μM = 12%) as well as H_1 histaminic receptor (% inh. at 1 μM = 6%) and M_1 muscarinic receptor (% inh. at 1 μM = 4%). Experiments toward selected "off-target" receptors were performed at Eurofins Scientific. These reduce a potential risk of undesired cardiovascular incidents (e.g., hypertension and/or arrhythmia) or CNS side effects (e.g., sedation).

Molecular Dynamics Simulations of the Interaction of Compound 7e, PZ-1444, and SAM-760 with the 5-HT$_6$R. Having identified structural elements responsible for different *in vitro* activities of imidazo[4,5-*c*]pyridine and imidazo[4,5-*b*]pyridine analogues, we further investigated the binding mode of two representative compounds, **7e** and PZ-1444, using molecular docking experiments (Figure 3). Additionally, to assess the impact of the central core, i.e., imidazo[4,5-*c*]pyridine *vs* benzimidazole moiety on the

https://dx.doi.org/10.1021/acs.jmedchem.0c02009
J. Med. Chem. 2021, 64, 1180−1196

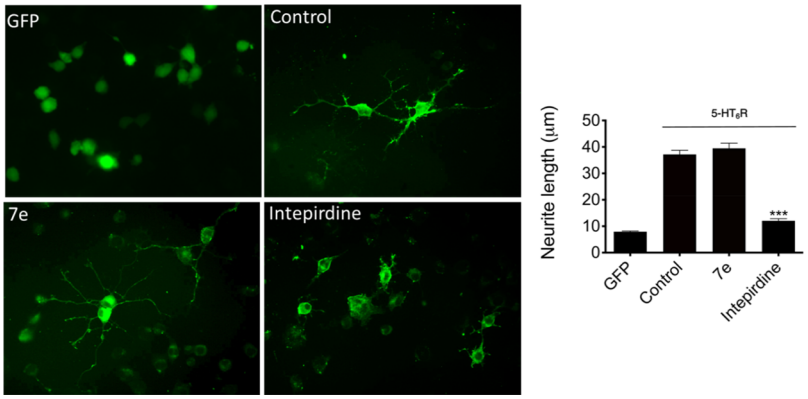

Figure 4. Evaluation of an impact of compound **7e** (1 mM) and intepirdine (1 mM) on neurite length in NG108-15 cells expressing a GFP-tagged 5-HT_6 receptor or GFP alone. Cells expressing the receptor were exposed to either DMSO (Control) or tested compounds for 24 h. Data were obtained from three independent experiments. The histogram presents the means ± SEM. ***$p < 0.001$ *vs.* cells expressing GFP.

ligand−5-HT_6R interaction, we also compared the binding mode of selected imidazopyridines with SAM-760, a benzimidazole derivative with a phenylsulfonyl fragment (Figure 4-SI). The binding mode was consistent with our previous study on different groups of 5-HT_6R ligands, using a homology model built on the β_2 adrenergic template (PDB ID: 4LDE).[39−43] The protonated piperazine moiety created a salt bridge with D3.32, the central core (imidazopyridine or benzimidazole) formed a CH−π interaction with F6.52/F6.51, and the terminal substituted phenyl ring fitted into a hydrophobic cavity formed by transmembrane domains (TMs) 3, 4, and 5 and extracellular loop 2 (ECL2). However, analysis of the binding modes obtained in the docking procedure, even for a set of receptor conformations, did not shed light on the potential explanation for the different pharmacological profiles of Gs signaling of compound **7e** and PZ-1444. Therefore, a series of 100 ns molecular dynamics (MD) simulations was performed using an initial geometry selected by visual inspection of the best binding modes. In order to facilitate analysis, trajectories obtained from MD simulations were clustered and the four most populated geometries were used for further analysis. The MD results indicated that PZ-1444 and compound **7e** retained key L−R interactions (D3.32, F6.51) but significantly changed the receptor conformation (Figure 3A). Calculated changes at the position of geometric centers of individual amino acids showed that the differences between conformations of the same complex selected from the clustering were small (green and blue lines on the graphs of the individual helices for the PZ-1444 and compound **7e** complexes, respectively, oscillate approximately 1 Å), while significant differences were visible between the conformations of both complexes (black line on the graphs of the individual helices). The largest changes (above 2 Å) within the binding pocket (areas marked in pink on the graphs of the individual helices) are visible in TMs 6, 5, and 4, while changes did not exceed 2 Å in the other TMs (except for three amino acids of TM 2, which has no direct interaction with the ligands). Moreover, compound SAM-760 bearing an unsubstituted phenylsulfonyl fragment showed changes at the position of geometric centers of individual amino acids within the binding pocket (TMs 6, 5, and 4) coherent to those observed for phenylsulfonyl derivative **7e**. On the contrary, *N*-benzyl imidazo[4,5-*b*]pyridine analog (PZ-1444) showed significant differences between conformations in MD trajectory clustering in comparison to **7e** and SAM-760 (Figure 3-SI). To finally confirm that the potential source of the differences between the MD simulations for the PZ-1444−receptor and compound **7e**−receptor complexes originates from the ligand structures, quantum mechanical calculations were performed. To investigate conformational preferences[44,45] of PZ-1444 and **7e**, a noncovalent interaction (NCI) approach was adapted. The isosurfaces of the reduced density gradient $s(r)$ were examined, and the resulting plots were generated (Figure 3B).

Within the structure of PZ-1444, only weak attractive noncovalent interactions were indicated. However, in compound **7e**, stronger $H_{12}\cdots N_3$ and $H_{20}\cdots N_5$ intramolecular hydrogen bonds between piperazine and imidazo[4,5-*c*]-pyridine moieties and weaker $H_8\cdots O_1$ and $H_5\cdots O_1$ hydrogen bonds between S=O and H−C of the *N*-ethyl substituent were observed. Such intramolecular hydrogen bonding in compound **7e** limits its flexibility during MD simulations, which probably causes a deviation of helices 6 and 4 from the binding site. Furthermore, the increased overall conformational flexibility of PZ-1444 compared to compound **7e** can be associated with the shifting of the nitrogen atom to the distal position of the pyridine ring of the imidazo[4,5-*b*]pyridine scaffold. This excludes the possibility of creating any intramolecular hydrogen bonds with the CH_2 group of the basic center. Therefore, the most populated conformation of PZ-1444 shows a twisting of the piperazine ring against the imidazo[4,5-*c*]pyridine plane.

Impact of Compound 7e on Neurite Growth. Previous studies have shown that the 5-HT_6R promotes neurite growth and neuronal differentiation through the agonist-independent activation of Cdk5, a protein kinase essential for a variety of functions in the developing brain.[6] These effects were initially demonstrated in the NG108-15 neuroblastoma cell line, a cellular model used for investigating neuronal differentiation mechanisms.[24] As previously described,[6] 5-HT_6R expression in NG108-15 cells induced an increase in neurite length, compared with cells expressing cytosolic GFP. Treatment of cells expressing the receptor with intepirdine (1 μM) led to a significant reduction in neurite length (12.06 ± 0.77 μm, n = 31 cells *vs.* 37.20 ± 1.53 μm, n = 32 in vehicle-treated cells). In contrast, compound **7e** (1 μM) did not affect the neurite length of NG108-15 cells (39.49 ± 1.95 μm, n = 31 cells, Figure 4). Since both PZ-1444[24] and **7e** did not influence neurite growth in this test, any type of substituent at the N^1

https://dx.doi.org/10.1021/acs.jmedchem.0c02009
J. Med. Chem. 2021, 64, 1180−1196

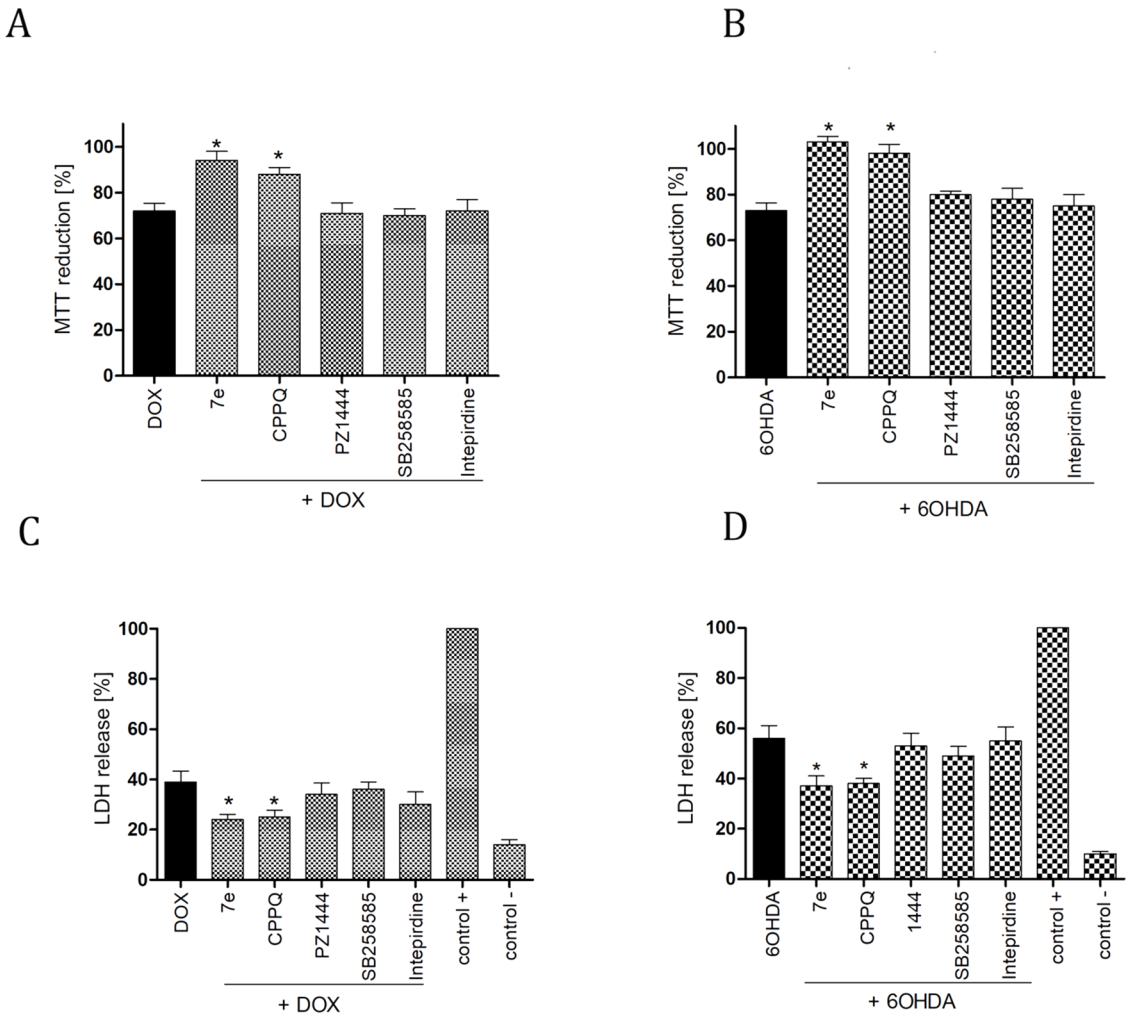

Figure 5. Glioprotective effects of 5-HT$_6$R antagonists. C8-D1A cell survival viability was determined using the MTT (A, B) and LDH assay (C, D). C8-D1A astrocytes were treated with either vehicle or compound **7e**, CPPQ, PZ-1444, SB258585, or intepirdine (all at 0.25 μM) for 5 h, and then DOX (10 μM) was added for the next 3 h, and cell viability was determined using MTT assay (A) or LDH assay (C). Alternatively, cells were exposed to the same compounds for 12 h, and subsequently 6-OHDA (25 μM) was exposed for the next 24 h, and cell viability was assessed using MTT assay (B) or LDH assay (D). Data were obtained from three independent experiments. Graphs present the means ± SD. $p < 0.05$ *vs.* cells treated with cytotoxic agents (DOX or 6-OHDA) using the Mann−Whitney test

position on imidazopyridine had no impact on agonist-independent 5-HT$_6$R-mediated Cdk5 signaling.

Glioprotective Effects of 5-HT$_6$R Antagonists. Glial cells, especially astrocytes, are responsible for maintaining brain homeostasis by releasing cytokines and growth factors, provisioning antioxidative molecules and modulating of extracellular ions.[46] Astrocytes play a crucial role in the initiation of the cell repair system as well as in preventing the glutamate excitotoxicity associated with some CNS diseases.[47] Thus, support of the neuroprotective functions of astrocytes might be considered an important strategy for enhancing neural survival and improving the current pharmacotherapy of neurodegenerative disorders.[48]

Expression of the 5-HT$_6$R in various neuronal populations is well documented,[49] but data concerning its expression and function in astrocytes remains limited. The 5-HT$_6$R mRNA was detected in cultured rat astrocytes.[50,51]

In line with these observations and our previous findings indicating that 5-HT$_6$R antagonists induce glioprotective effects,[39] we next sought to evaluate the impact of compound **7e**, in comparison with other previously described 5-HT$_6$R antagonists, on the survival of C8-D1A astrocyte cell line derived from the mouse cerebellum. For this purpose, we selected compounds from various chemotypes, which behave as neutral antagonists (compound **7e**, CPPQ),[12] or inverse agonists (PZ-1444, SB258585, and intepirdine) at Gs signaling.[24,52,53] The expression of 5-HT$_6$R in C8-D1A astrocytes was first confirmed using *in vitro* [^{3}H]-LSD binding (Figure 5-SI).

We then explored the influence of the tested compounds on astrocyte cell viability using the MTT (3-[4,5-dimethylthiazol-2-yl]-2,5-diphenyl tetrazolium bromide) assay, as a widely accepted approach to screen for drug cytotoxicity. At the concentration of 0.25 μM, none of the evaluated compounds showed a significant effect on C8-D1A cell viability and each displayed a CC_{50} (cytotoxic concentration) higher than 1 μM, indicating a lack of toxicity toward CNS cells at concentrations exhibiting pharmacological activity. We next examined the glioprotective properties of the tested compounds (**7e**, CPPQ, PZ-1444, SB-258585, and intepirdine) against DOX/6-OHDA-induced toxicity in C8-D1A astrocytes.

https://dx.doi.org/10.1021/acs.jmedchem.0c02009
J. Med. Chem. 2021, 64, 1180−1196

Cells were pre-incubated with the test compounds, and then the toxins DOX or 6-OHDA were added to the cells to induce cell injury for an additional 3 h and 24 h incubation period, respectively. Compound **7e** and CPPQ protected the cells against DOX- and 6-OHDA-induced cytotoxicity, whereas neither PZ-1444, SB258585, nor intepirdine induced a protective effect (Figure 5A,B). These results were corroborated in lactate dehydrogenase (LDH) test, an assay that determines cell membrane integrity (Figures 5C and 5D for DOX- and 6-OHDA-induced cytotoxicity, respectively). In view of these findings, the glioprotection produced by compound **7e** and CPPQ could result from the different receptor conformations upon binding to neutral antagonists *vs.* inverse agonists. More detailed experiments aimed to further study the stabilization of the constitutively active state of 5-HT_6R by neutral antagonists in the glioprotection process are warranted.

Pro-cognitive Properties of Compound 7e. Finally, the impact of compound **7e** on short-term memory was examined in the NOR test. As expected, rats treated with vehicle, but not with scopolamine (SCOP, 1.25 mg/kg), spent significantly more time exploring the novel object than the familiar one, indicating that the anti-muscarinic agent abolished the ability to discriminate between novel and familiar objects. This deficit was fully rescued after a single *p.o.* administration of compound **7e** at a dose of 3 mg/kg, but not 1 mg/kg (Figure 6).

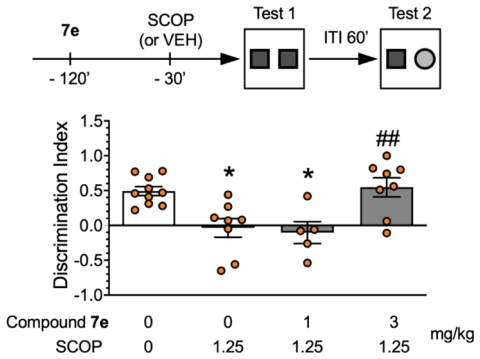

Figure 6. Effects of compound **7e** on scopolamine-induced cognitive impairment in the NOR test in rats. The data represent the means ± SEM of the discrimination index (DI) measured in $N = 5–10$ animals per group. Symbols: $^{*}p < 0.05$ *vs.* vehicle-treated group; $^{\#\#}p < 0.01$ *vs.* scopolamine (SCOP)-treated group, Tukey's multiple comparison post-hoc test following ANOVA: $F(3,27) = 7.879$, $P < 0.001$.

It is difficult to directly compare pro-cognitive effects produced by targeting agonist-induced 5-HT_6R states (i.e., neutral antagonists) and constitutively active states of 5-HT_6R (i.e., inverse agonists) based on active doses in *in vivo* setting. It appears that compound **7e**, which behaves as a neutral antagonist and contains the N^1-phenylsulfonyl moiety, fully prevented deficits in the NOR test at a higher dose (3 mg/kg) than PZ-1444, which behaves as an inverse agonist and contains the N^1-benzyl moiety (1 mg/kg).[24]

These findings corroborate previous observations from our laboratory made with CPPQ[12] and suggest that 5-HT_6R neutral antagonists administration may prevent debilitating effects of the *N*-methyl-D-aspartate (NMDA) receptor antagonist phencyclidine (PCP) or the muscarinic receptor antagonist scopolamine, thus reproducing the pro-cognitive effects of inverse agonists of 5-HT_6R.

CONCLUSIONS

The study presents a structure-based approach to explore the impact of N^1-benzyl and N^1-phenylsulfonyl fragments in imidazo[4,5-*c*]pyridine analogues of PZ-1444 (a 5-HT_6R inverse agonist at the Gs signaling pathway), regarding their properties on receptor-dependent Gs and Cdk5 signaling. Selected imidazo[4,5-*c*]pyridines, containing N^1-phenylsulfonyl moieties, with compound **7e** (PZ-1727) as the lead, behave as neutral antagonists at Gs signaling. Consistent with this result, molecular dynamics simulations identified significant conformational changes in the 5-HT_6R-ligand complexes, especially for TMs 4, 5, and 6, which contributed to the different functional profiles of compound **7e** and PZ-1444. To the best of our knowledge, this is the first time that such experiments have been reported with 5-HT_6R modulators. It was also found that compound **7e** and CPPQ reduce the cytotoxicity of doxorubicin and 6-OHDA in C8-D1A astrocytes, suggesting a potential role of astrocytic 5-HT_6Rs linked to their protective action against astrocyte injury. Notably, this effect was not observed after treatment with 5-HT_6R inverse agonists (PZ-1444, SB258585, and intepirdine). Considering the challenges in developing clinically valid therapies, compound **7e**, which reverses scopolamine-induced cognitive impairment in the NOR test and displays glioprotective properties, can be considered a molecular tool to investigate the role of the 5-HT_6R in neurodegenerative and psychiatric disorders.

EXPERIMENTAL SECTION

Chemistry. *General Methods.* Solvents and chemicals were purchased from Sigma-Aldrich and Acros. The LC/MS analyses were recorded using a UHPLC/MS Waters system consisting of a UHPLC Acquity chromatograph and single quadrupole mass spectrometer (for more information, see the Supporting Information). The UHPLC/MS purity of all the final compounds was confirmed to be 95% or higher. HRMS analysis was obtained by LC/MS and using an Orbitrap Elite high-resolution mass spectrometer (Dionex Ultimate 3000, Thermo Exactive plus, MA, USA). For more information, see the Supporting Information. All ^{1}H and ^{13}C NMR experiments were acquired using JEOL ECA400II or ECX500 spectrometers (for more information, see the Supporting Information). Chemical shifts (δ) are reported in parts per million (ppm), and coupling constants (J) are reported in Hertz (Hz).

*General Procedures. Preparation of 2-Chloro-3-nitropyridin-4-amine (**2**).* 2,4-Dichloro-3-nitropyridine 1 (3.7 g; 19 mmol) in DMSO (25 mL) was heated up to 80 °C. After that, ammonium hydroxide solution (25% aq, 2 mL) was added to the solution every 15 min in a total of four portions. After the addition of the fourth portion, a higher volume of ammonium hydroxide solution (25% aq, 3 mL) was added and the mixture reaction was stirred for 1 h. After cooling the reaction mixture, water (75 mL) was added, resulting in precipitation of a yellow solid. This solid was filtered and washed with water, and the product was crystallized from methanol, resulting in 2.44 g of a yellow powder (yield 74%).

*Preparation of tert-Butyl 4-(4-Amino-3-nitropyridin-2-yl)-piperazine-1-carboxylate (**3**).* A mixture of **2** (1 g; 5.8 mmol), *N*-Boc-piperazine (1.62 g; 8.7 mmol), and DIEA (1.52 mL; 8.7 mmol) in DMSO (25 mL) was reacted at 80 °C for 2 h. Then, the mixture was cooled to room temperature, and 50 mL of water was added, followed by extracting with EtOAc (2 × 50 mL), washing with water (3 × 50 mL), drying over Na_2SO_4, and concentrating under reduced pressure. The product was crystallized from a mixture of methanol and water, providing 1.50 g of the product (yield 80%).

*Preparation of tert-Butyl 4-(3,4-Diaminopyridin-2-yl)piperazine-1-carboxylate (**4**).* To a solution of **3** (1.78 g; 5.5 mmol) in degassed EtOH (25 mL), 100 mg of 10% Pd/C was added. A balloon with a

https://dx.doi.org/10.1021/acs.jmedchem.0c02009
J. Med. Chem. 2021, 64, 1180−1196

needle containing hydrogen was put into the rubber septum on the flask to saturate a mixture with hydrogen. After 15 min, a needle was pulled up above the solution and the mixture was left to stir for 16 h. The catalyst was then filtered, and the solution was evaporated to obtain 1.55 g of the crude product (yield 96%), which was used for the next step without further purification.

*Preparation of Imidazo[4,5-c]pyridine (**5a**).* A mixture containing **4** (1 g; 3.4 mmol) and triethyl orthoformate (5 mL) in DMSO (5 mL) was reacted at 100 °C for 1 h. The mixture was cooled to room temperature and quenched upon addition of 50 mL of water. The reaction mixture was then extracted with EtOAc (2 × 50 mL) followed by washing with water (3 × 50 mL), drying over Na_2SO_4, filtering, and freeze-drying. The product was purified *via* crystallization in a mixture of methanol and water, yielding 0.63 g (61%).

*Preparation of Imidazo[4,5-c]pyridines (**5b**–**d**).* A mixture of **4** (1 g; 3.4 mmol) and aldehyde (10.2 mmol; 3 eq) in DMF (10 mL) was stirred at 90 °C for 16 h. After cooling to room temperature and addition of water (20 mL), the mixture was extracted with EtOAc (2 × 25 mL), washed with water (3 × 25 mL), dried over Na_2SO_4, filtered, and evaporated. The product was purified *via* crystallization (in MeOH:H_2O) or *via* column chromatography (DCM:MeOH, 9.5:0.5), with high yields (70–74%).

*Preparation of N-Boc-N-Phenylsulfonyl-1H-imidazo[4,5-c]-pyridines (**6a**–**n**).* A mixture of **5a**–**d** (0.3 mmol) and BTPP (138 μL; 0.45 mmol) in DCM (1 mL) was cooled to 0 °C. After 15 min, the corresponding benzenesulfonyl chloride (0.45 mmol, 1.5 eq) was added. The reaction mixture was left to heat from 0 °C to room temperature in the interval of 16 h. After that, water (5 mL) and DCM (4 mL) were added. The organic fraction was isolated, and the aqueous fraction was washed with DCM (5 mL). Merged organic fractions were additionally washed with water (3 × 5 mL), dried over Na_2SO_4, filtered, and evaporated. The product was crystallized from a mixture of methanol and water or *via* column chromatography (DCM:MeOH, 9.5:0.5). Yields ranged between 40 and 90%.

*Preparation of N-Phenylsulfonyl-1H-imidazo[4,5-c]pyridine Acetates (**7a**–**n**).* Compounds **6a**–**n** (100 mg) were dissolved in 10% TFA in DCM (1.5 mL) and stirred for 2 h at room temperature. After the completion, DCM (3.5 mL) and water (5 mL) were added to the reaction mixture. The aqueous phase was separated, and the organic phase was washed with water (2 × 5 mL). The combined aqueous layers were neutralized with Na_2CO_3 to slight basic pH (∼8). Then, the solution was extracted with DCM (4 × 5 mL), and the organic phase was evaporated to obtain the product as a free base. The evaporated residue was then treated with acetic acid (2 mL) for 30 min. After evaporating acetic acid, the sample was evaporated multiple times (3–5 times) from acetonitrile to obtain a solid residue. These were suspended in acetonitrile, filtered, and dried to provide final products (yield varied between 30 and 80%).

*Preparation of tert-Butyl 4-(2-Amino-3-nitropyridin-4-yl)-piperazine-1-carboxylate (**9**).* 2-Amino-3-nitro-4-chloropyridine **8** (300 mg; 1.74 mmol), Boc-piperazine (360 mg; 1.9 mmol) and DIEA (330 μL; 1.9 mmol) were dissolved in DMSO (5 mL). This solution was stirred at room temperature for 3 h. Then, it was quenched with water (25 mL), extracted with EtOAc (2 × 25 mL), washed with water (3 × 50 mL), dried over Na_2SO_4, filtered, and evaporated. The pure product was obtained *via* crystallization methanol and water, yielding 320 mg of the product (yield 57%).

*Preparation of tert-Butyl 4-(2,3-Diaminopyridin-4-yl)piperazine-1-carboxylate (**10**).* Compound **9** (310 mg; 0.96 mmol) was dissolved in EtOH (7 mL), and 10% Pd/C (100 mg) was added. A balloon with a needle containing hydrogen was put into the rubber septum on the flask, and the reaction mixture was left to saturate with hydrogen for 15 min. After that, a needle was pulled up above the solution and the mixture was left to stir for 16 h. The catalyst was filtered, and the solution was evaporated to obtain 231 mg of the crude product (yield 82%).

*Preparation of Imidazo[4,5-b]pyridine (**11**).* A mixture of **10** (189 mg; 0.64 mmol) and isobutyraldehyde (176 μL; 1.93 mmol) in DMF (4 mL) was reacted at 90 °C for 16 h. The sample was quenched with water (10 mL) and extracted with EtOAc (2 × 10 mL). Then, the organic fraction was additionally washed with water (3 × 20 mL), dried over Na_2SO_4, filtered, and evaporated. The pure product was obtained *via* column chromatography (DCM:MeOH, 9:1), giving 113 mg of the product (yield 51%).

*Preparation of N-Phenylsulfonyl-1H-imidazo[4,5-b]pyridines (**12**).* A mixture of **11** (100 mg; 0.289 mmol) and BTPP (106 μL; 0.347 mmol) in DCM (1 mL) was cooled to 0 °C. After 15 min, benzenesulfonyl chloride (1.2 eq) was added. The reaction mixture was left to heat from 0 °C to room temperature in the interval of 16 h. After that, water (5 mL) and DCM (4 mL) were added. The organic layer was separated, and the aqueous layer was washed with DCM (5 mL). Combined organic layers were washed with water (3 × 5 mL), dried over Na_2SO_4, filtered, and evaporated. The crude product was detected by UHPLC-MS but decomposed during silica gel purification or recrystallization from methanol.

*Characterization of Final Compounds (**7a**–**n**). 1-(Phenylsulfonyl)-4-(piperazin-1-yl)-1H-imidazo[4,5-c]pyridine Acetate (**7a**).* White solid, yield 79%; UHPLC-UV purity 99+% (220 nm); $C_{18}H_{21}N_5O_4S$, MW 403.46. ^{1}H NMR (500 MHz, CD_3OD) δ ppm: 1.92 (s, 3H), 3.19–3.23 (m, 4H), 4.22–4.26 (m, 4H), 7.33 (d, *J* = 5.7 Hz, 1H), 7.62–7.66 (m, 2H), 7.73–7.78 (m, 1H), 8.04 (d, *J* = 5.7 Hz, 1H), 8.12–8.15 (m, 2H), 8.57 (s, 1H). ^{13}C NMR (125 MHz, CD_3OD) δ ppm: 23.4, 44.9, 45.4, 101.2, 128.8, 129.7, 131.3, 136.7, 138.5, 139.4, 140.1, 144.4, 152.4; mp 132–140 °C; HRMS (ESI-TOF) *m*/*z* calculated for $C_{16}H_{18}N_5O_2S^+$ [M + H$^+$] 344.1176, found 344.1189.

*1-((3-Chlorophenyl)sulfonyl)-4-(piperazin-1-yl)-1H-imidazo[4,5-c]pyridine Acetate (**7b**).* White solid, yield 34%; UHPLC-UV purity 99+% (220 nm); $C_{18}H_{20}ClN_5O_4S$, MW 437.90. ^{1}H NMR (500 MHz, CD_3OD) δ ppm: 1.92 (s, 3H), 3.17–3.22 (m, 4H), 4.21–4.26 (m, 4H), 7.33 (d, *J* = 5.7 Hz, 1H), 7.63 (t, *J* = 8.0 Hz, 1H), 7.77 (dd, *J* = 7.7, 1.4 Hz, 1H), 8.06 (d, *J* = 5.7 Hz, 1H), 8.08 (dd, *J* = 8.0, 1.2 Hz, 1H), 8.19 (s, 1H), 8.59 (s, 1H). ^{13}C NMR (125 MHz, CD_3OD) δ ppm: 23.6, 45.0, 45.6, 100.9, 127.3, 128.5, 129.6, 133.0, 136.8, 137.3, 139.3, 140.0, 140.2, 144.7, 152.5; mp 125–126 °C; HRMS (ESI-TOF) *m*/*z* calculated for $C_{16}H_{17}ClN_5O_2S^+$ [M + H$^+$] 378.0786, found 378.0791.

*1-((3-Fluorophenyl)sulfonyl)-4-(piperazin-1-yl)-1H-imidazo[4,5-c]pyridine Acetate (**7c**).* White solid, yield 73%; UHPLC-UV purity 99+% (220 nm); $C_{18}H_{20}FN_5O_4S^+$, MW 421.45. ^{1}H NMR (500 MHz, CD_3OD) δ ppm: 1.92 (s, 3H), 3.17–3.21 (m, 4H), 4.21–4.25 (m, 4H), 7.50–7.57 (m, 1H), 7.65–7.72 (m, 1H), 7.94–8.01 (m, 2H), 8.05 (d, *J* = 5.7 Hz, 1H), 8.58 (s, 1H). ^{13}C NMR (125 MHz, CD_3OD) δ ppm: 23.6, 45.0, 45.6, 101.0, 116.0 ($^2J_{C-F}$ = 25.8 Hz), 123.9 ($^2J_{C-F}$ = 21.9 Hz) 125.0 ($^4J_{C-F}$ = 3.6 Hz), 129.6, 133.7 ($^3J_{C-F}$ = 7.8 Hz), 139.3, 140.0, 140.3 ($^3J_{C-F}$ = 7.5 Hz), 144.7, 152.5, 164.1 ($^1J_{C-F}$ = 251.6 Hz), 179.5; mp 130–132 °C; HRMS (ESI-TOF) *m*/*z* calculated for $C_{16}H_{17}FN_5O_2S^+$ [M + H$^+$] 362.1082, found 362.1080.

*1-((3-Methoxyphenyl)sulfonyl)-4-(piperazin-1-yl)-1H-imidazo-[4,5-c]pyridine Acetate (**7d**).* White solid, yield 33%; UHPLC-UV purity 99+% (220 nm); $C_{19}H_{23}ClN_5O_5S$, MW 433.48. ^{1}H NMR (500 MHz, CD_3OD) δ ppm: 1.92 (s, 3H), 3.18–3.21 (m, 4H), 3.85 (s, 3H), 4.21–4.25 (m, 4H), 7.27–7.31 (m, 1H), 7.33 (d, *J* = 5.7 Hz, 1H), 7.54 (t, *J* = 8.2 Hz, 1H), 7.59 (t, *J* = 2.2 Hz, 1H), 7.66–7.70 (m, 1H), 8.04 (d, *J* = 5.7 Hz, 1H), 8.58 (s, 1H). ^{13}C NMR (125 MHz, CD_3OD) δ ppm: 23.6, 45.0, 45.5, 56.6, 101.1, 113.6, 120.7, 122.4, 129.6, 132.5, 139.4, 139.5, 140.2, 144.4, 152.5, 162.1, 179.5; mp 117–119 °C; HRMS (ESI-TOF) *m*/*z* calculated for $C_{17}H_{20}ClN_5O_3S^+$ [M + H$^+$] 374.1281, found 374.1286.

*1-((3-Chlorophenyl)sulfonyl)-2-ethyl-4-(piperazin-1-yl)-1H-imidazo[4,5-c]pyridine Acetate (**7e**).* White solid, yield 64%; UHPLC-UV purity 99% (220 nm); $C_{20}H_{24}ClN_5O_4S$, MW 465.95. ^{1}H NMR (500 MHz, CD_3OD) δ ppm: 1.40 (t, *J* = 7.3 Hz, 3H), 1.92 (s, 3H), 3.13–3.19 (m, 2H), 3.19–3.23 (m, 4H), 4.21–4.25 (m, 4H), 7.43 (d, *J* = 6.0 Hz, 1H), 7.58–7.65 (m, 1H), 7.74–7.79 (m, 1H), 7.91–7.96 (m, 1H), 7.99–8.04 (m, 2H). ^{13}C NMR (125 MHz, CD_3OD) δ ppm: 12.1, 24.3, 45.1, 45.8, 102.3, 126.7, 127.9, 133.1, 136.7, 137.2, 141.0, 141.7, 144.00, 154.7; mp 126–128 °C; HRMS (ESI-TOF) *m*/*z* calculated for $C_{18}H_{21}ClN_5O_2S^+$ [M + H$^+$] 406.1099, found 406.1098.

https://dx.doi.org/10.1021/acs.jmedchem.0c02009
J. Med. Chem. 2021, 64, 1180–1196

*2-Ethyl-1-((3-fluorophenyl)sulfonyl)-4-(piperazin-1-yl)-1H-imidazo[4,5-c]pyridine Acetate (**7f**).* White solid, yield 48%; UHPLC-UV purity 98% (220 nm); $C_{20}H_{24}FN_5O_4S$, MW 449.50. ^{1}H NMR (500 MHz, CD_3OD) δ ppm: 1.40 (t, J = 7.3 Hz, 3H), 1.92 (s, 3H), 3.14−3.19 (m, 2H), 3.19−3.22 (m, 4H), 4.18−4.25 (m, 4H), 7.43 (d, J = 5.7 Hz, 1H), 7.48−7.55 (m, 1H), 7.67 (td, J = 8.2, 5.2 Hz, 1H), 7.80 (dt, J = 7.9, 2.2 Hz, 1H), 7.85 (dd, J = 8.0, 0.9 Hz, 1H), 8.02 (d, J = 5.7 Hz, 1H). ^{13}C NMR (125 MHz, CD_3OD) δ ppm: 12.0, 24.1, 44.9, 45.7, 102.2, 115.3 ($^2J_{C-F}$ = 25.2 Hz), 123.6 ($^2J_{C-F}$ = 21.6 Hz), 124.3 ($^4J_{C-F}$ = 3.6 Hz), 127.7, 133.6 ($^3J_{C-F}$ = 8.4 Hz), 143.8, 151.9, 154.5 ($^1J_{C-F}$ and second $^3J_{C-F}$ not detected in the spectrum due to the low concentration of the sample). HRMS (ESI-TOF) m/z calculated for $C_{18}H_{21}FN_5O_2S^+$ [M + H$^+$] 390.1395, found 390.1395.

*2-Isopropyl-1-(phenylsulfonyl)-4-(piperazin-1-yl)-1H-imidazo-[4,5-c]pyridine Acetate (**7g**).* White solid, yield 42%; UHPLC-UV purity 99 + % (220 nm); $C_{21}H_{27}N_5O_4S$, MW 445.54. ^{1}H NMR (500 MHz, CD_3OD) δ ppm: 1.34 (d, J = 6.6 Hz, 6H), 1.88−1.94 (m, 3H), 3.18−3.26 (m, 4H), 3.77−3.88 (m, 1H), 4.14−4.25 (m, 4H), 7.49 (d, J = 5.7 Hz, 1H), 7.59−7.67 (m, 2H), 7.70−7.79 (m, 1H), 7.92−8.05 (m, 3H). ^{13}C NMR (125 MHz, CD_3OD) δ ppm: 22.8, 23.6, 29.8, 45.0, 45.7, 102.8, 128.2, 131.3, 136.6, 139.6, 141.6, 143.7, 152.0, 159.0; mp 125−130 °C; HRMS (ESI-TOF) m/z calculated for $C_{19}H_{24}N_5O_2S^+$ [M + H$^+$] 386.1645, found 386.1648.

*1-((3-Chlorophenyl)sulfonyl)-2-isopropyl-4-(piperazin-1-yl)-1H-imidazo[4,5-c]pyridine Acetate (**7h**).* White solid, yield 43%; UHPLC-UV purity 99% (220 nm); $C_{21}H_{26}ClN_5O_4S$, MW 479.98. ^{1}H NMR (500 MHz, CD_3OD) δ ppm: 1.36 (d, J = 6.9 Hz, 6H), 1.92 (s, 3H), 3.18−3.22 (m, 4H), 3.78−3.86 (m, 1H), 4.18−4.25 (m, 4H), 7.46 (d, J = 6.0 Hz, 1H), 7.60−7.64 (m, 1H), 7.76−7.79 (m, 1H), 7.90−7.93 (m, 1H), 8.00 (t, J = 2.0 Hz, 1H), 8.03 (d, J = 5.7 Hz, 1H). ^{13}C NMR (125 MHz, CD_3OD) δ ppm: 22.8, 23.7, 30.0, 45.0, 45.9, 102.5, 126.6, 127.8, 133.1, 136.7, 137.2, 141.5, 144.0, 152.0, 158.9; mp 96−101 °C; HRMS (ESI-TOF) m/z calculated for $C_{19}H_{23}ClN_5O_2S^+$ [M + H$^+$] 420.1255, found 420.1260.

*1-((3-Fluorophenyl)sulfonyl)-2-isopropyl-4-(piperazin-1-yl)-1H-imidazo[4,5-c]pyridine Acetate (**7i**).* White solid, yield 44%; UHPLC-UV purity 99+% (220 nm); $C_{21}H_{26}FN_5O_4S$, MW 463.53. ^{1}H NMR (500 MHz, CD_3OD) δ ppm: 1.36 (d, J = 6.9 Hz, 6H), 1.92 (s, 3H), 3.18−3.23 (m, 4H), 3.78−3.87 (m, 1H), 4.19−4.25 (m, 4H), 7.47 (d, J = 5.7 Hz, 1H), 7.50−7.57 (m, 1H), 7.64−7.70 (m, 1H), 7.77−7.84 (m, 2H), 8.02 (d, J = 5.7 Hz, 1H). ^{13}C NMR (125 MHz, CD_3OD) δ ppm: 22.8, 23.7, 29.9, 45.0, 45.7, 102.6, 115.4 ($^2J_{C-F}$ = 25.2 Hz), 123.8 ($^2J_{C-F}$ = 21.6 Hz), 124.3 ($^4J_{C-F}$ = 3.6 Hz), 127.9, 133.7 ($^3J_{C-F}$ = 7.2 Hz), 141.5, 144.0, 152.0, 158.9 ($^1J_{C-F}$ and second $^3J_{C-F}$ not detected in the spectrum due to the low concentration of the sample); mp 97−100 °C; HRMS (ESI-TOF) m/z calculated for $C_{19}H_{23}FN_5O_2S^+$ [M + H$^+$] 404.1551, found 404.1552.

*2-Isopropyl-1-((3-methoxyphenyl)sulfonyl)-4-(piperazin-1-yl)-1H-imidazo[4,5-c]pyridine Acetate (**7j**).* White solid, yield 30%; UHPLC-UV purity 99+% (220 nm); $C_{22}H_{29}N_5O_5S$, MW 475.56. ^{1}H NMR (500 MHz, CD_3OD) δ ppm: 1.35 (d, J = 6.9 Hz, 6H), 1.92 (s, 3H), 3.17−3.25 (m, 4H), 3.80−3.88 (m, 4H), 4.17−4.25 (m, 4H), 7.27−7.32 (m, 1H), 7.40−7.44 (m, 1H), 7.48 (d, J = 6.0 Hz, 1H), 7.50−7.56 (m, 2H), 8.0 (d, J = 6.0 Hz, 1H). ^{13}C NMR (125 MHz, CD_3OD) δ ppm: 22.8, 23.6, 29.8, 45.0, 45.8, 56.6, 102.8, 113.1, 119.9, 122.1, 128.0, 132.6, 140.6, 141.6, 143.7, 152.0, 159.0, 162.0; mp 115−123 °C; HRMS (ESI-TOF) m/z calculated for $C_{20}H_{26}N_5O_3S^+$ [M + H$^+$] 416.1751, found 416.1751.

*2-Phenyl-1-(phenylsulfonyl)-4-(piperazin-1-yl)-1H-imidazo[4,5-c]pyridine Acetate (**7k**).* White solid, yield 56%; UHPLC-UV purity 96% (220 nm); $C_{24}H_{25}N_5O_4S$, MW 479.56. ^{1}H NMR (500 MHz, CD_3OD) δ ppm: 1.92 (s, 3H), 3.13−3.25 (m, 4H), 4.11−4.26 (m, 4H), 7.39−7.56 (m, 8H), 7.56−7.61 (m, 1H), 7.62 (d, J = 5.7 Hz, 1H), 7.64−7.69 (m, 1H), 8.11 (d, J = 6.0 Hz, 1H). ^{13}C NMR (125 MHz, CD_3OD) δ ppm: 23.6, 45.0, 45.7, 101.5, 103.5, 128.4, 128.5, 129.0, 130.9, 131.1, 132.0, 132.2, 136.5, 139.0, 142.5, 144.4, 152.2, 152.5. HRMS (ESI-TOF) m/z calculated for $C_{22}H_{22}N_5O_2S^+$ [M + H$^+$] 420.1489, found 420.1493.

*1-((3-Chlorophenyl)sulfonyl)-2-phenyl-4-(piperazin-1-yl)-1H-imidazo[4,5-c]pyridine Acetate (**7l**).* White solid, yield 76%; UHPLC-UV purity 98% (220 nm); $C_{24}H_{24}ClN_5O_4S$, MW 514.00. ^{1}H NMR (500 MHz, CD_3OD) δ ppm: 1.92 (s, 3H), 3.19−3.23 (m, 4H), 4.18−4.24 (m, 4H), 7.32−7.36 (m, 1H), 7.44−7.47 (m, 2H), 7.50 (d, J = 4.3 Hz, 4H), 7.59−7.64 (m, 2H), 7.66−7.70 (m, 1H), 8.13 (d, J = 5.7 Hz, 1H). ^{13}C NMR (125 MHz, CD_3OD) δ ppm: 23.4, 45.0, 45.6, 103.3, 126.7, 128.4, 129.1, 130.7, 132.2, 132.7, 136.6, 140.4, 142.4, 144.6, 151.9, 152.5; mp 137−140 °C; HRMS (ESI-TOF) m/z calculated for $C_{22}H_{21}ClN_5O_2S^+$ [M + H$^+$] 454.1099, found 454.1098.

*1-((3-Fluorophenyl)sulfonyl)-2-phenyl-4-(piperazin-1-yl)-1H-imidazo[4,5-c]pyridine Acetate (**7m**).* White solid, yield 62%; UHPLC-UV purity 99% (220 nm); $C_{24}H_{24}FN_5O_4S$, MW 497.55. ^{1}H NMR (500 MHz, CD_3OD) δ ppm: 1.93 (s, 3H), 3.24−3.27 (m, 4H), 4.21−4.28 (m, 4H), 7.16−7.20 (m, 1H), 7.33−7.38 (m, 1H), 7.43−7.47 (m, 1H), 7.48−7.54 (m, 5H), 7.59−7.64 (m, 2H), 8.14 (d, J = 6.0 Hz, 1H). ^{13}C NMR (125 MHz, CD_3OD) δ ppm: 22.9, 44.8, 45.3, 103.4, 115.7 ($^2J_{C-F}$ = 26.4 Hz), 123.7 ($^2J_{C-F}$ = 21.6 Hz), 124.5 ($^4J_{C-F}$ = 3.6 Hz), 128.4, 129.1, 130.8, 132.2, 133.3 ($^3J_{C-F}$ = 8.4 Hz), 142.5, 144.6, 152.1, 152.3, 163.8 ($^1J_{C-F}$ = 251.9 Hz), 178.6 (second $^3J_{C-F}$ not detected in the spectrum due to the low concentration of the sample); mp 126−128 °C; HRMS (ESI-TOF) m/z calculated for $C_{22}H_{21}FN_5O_2S^+$ [M + H$^+$] 438.1395, found 438.1379.

*1-((3-Methoxyphenyl)sulfonyl)-2-phenyl-4-(piperazin-1-yl)-1H-imidazo[4,5-c] pyridine Acetate (**7n**).* White solid, yield 71%; UHPLC-UV purity 99% (220 nm); $C_{25}H_{27}N_5O_5S$, MW 509.58. ^{1}H NMR (500 MHz, CD_3OD) δ ppm: 1.92 (s, 3H), 3.18−3.23 (m, 4H), 3.70 (s, 3H), 4.14−4.25 (m, 4H), 6.86−6.92 (m, 1H), 7.09−7.14 (m, 1H), 7.16−7.22 (m, 1H), 7.33−7.40 (m, 1H), 7.45−7.56 (m, 4H), 7.57−7.64 (m, 2H), 8.04−8.15 (m, 1H). ^{13}C NMR (125 MHz, CD_3OD) δ ppm: 23.6, 45.0, 45.8, 56.4, 103.5, 113.0, 120.3, 122.5, 128.5, 129.0, 131.1, 132.0, 132.1, 132.3, 139.9, 142.5, 144.4, 152.2, 152.5, 161.6; mp 132−135 °C; HRMS (ESI-TOF) m/z calculated for $C_{23}H_{24}N_5O_3S^+$ [M + H$^+$] 450.1594, found 450.1565.

***In Silico* Simulations.** *pKa Calculation.* pK_a values calculations were performed for the lowest energy conformations for each compound (minimization performed in macroModel)[54] in water as a solvent using Jaguar.[55,56] The default settings were used, i.e., the energy change at level of 5 × 10^{-05}, no SCF level shift, no thermal smearing, and ultrafine accuracy level.

Molecular Docking. The 5-HT$_6$R homology models built on the β_2 receptor template (PDB ID: 4LDE), successfully applied in our earlier studies of different groups of 5-HT$_6$R ligands, were used in this study.[42,57] In order to tune the conformation of the receptor to the studied compounds, the induced-fit docking (IFD) procedure from the Schrödinger package was used. The three-dimensional structures of the ligands were obtained using LigPrep v3.6,[58] and the appropriate ionization states at pH = 7.4 ± 1.0 were assigned using Epik v3.4.[59] The Protein Preparation Wizard was used to assign the bond orders and appropriate amino acid ionization states and to check for steric clashes. The receptor grid was generated (OPLS3 force field)[60] by centering the grid box with a size of 12 Å on the D3.32 side chain. Automated flexible docking was performed using Glide v6.9[61] at the SP level, and 10 poses per ligand were generated.

Molecular Dynamics Simulations. A 100 ns-long molecular dynamics (MD) simulations were performed using Desmond software from Schrödinger Suite. Each ligand−protein complex was placed in a two-layer POPC membrane (300 K), in which the position was calculated using a PPM web server (accessed 26-01-2020). Next, the system was solvated (the TIP4P potential was used), all atoms were parametrized (the OPLS3 force field), and the ionic strength was added (the 0.15 M concentration of NaCl). The MD trajectories were clustered (the hierarchical clustering method and 10 final clusters) using trajectory analysis tools from Maestro Schrödinger Suite. Among all clusters, the four top-rated were selected for further analysis.

Monitoring Changes in Receptor Conformation. In order to monitor changes occurring in individual fragments of the 5-HT$_6$R helix during molecular dynamics of receptor-PZ-1444, compound **7e**, and SAM-760 complexes, the spatial coordinates (x,y,z) of atoms belonging to particular amino acids were converted into single points

https://dx.doi.org/10.1021/acs.jmedchem.0c02009
J. Med. Chem. 2021, 64, 1180−1196

corresponding to their geometric center (i.e., centroid). This approximation allows one to track amino acid position changes by considering the trajectory of one point. The differences between receptor conformations were determined by calculating the Euclidean distance between centroids of the same amino acids.

Theoretical Calculations. To recognize intramolecular interactions within the PZ-1444, compound **7e**, and SAM-760 structural frameworks, the NCIPLOT program was used.[58] First, the density functional theory (DFT) calculations for ligand conformations determined from the MD trajectory (the most populated cluster) with the GAUSSIAN16 package at the B3LYP-D3/6-311G(d,p) level were performed.[59] Wave functions were obtained using the 6-311G** basis set and further used to generate reduced electron density gradient (RDG) surfaces by means of the NCIPLOT program. The NCI (non-covalent interaction) analysis is based on the reduced RDG defined as

$$s(r) = \frac{|\nabla\rho(r)|}{2(3\pi)^{1/3}\rho(r)^{4/3}}$$

where $\nabla\rho(r)$ corresponds to a gradient of the electron density. The NCI allows visualization of both attractive and repulsive interaction regions. If a molecule contains the non-covalent interaction, a characteristic spike in low-gradient and low-density regions (absent for covalent bonds) on scatterplots of $s(r)$ *vs.* $\rho(r)$ appeared. Additionally, taking the sign of the second eigenvalue (λ_2) of the Hessian matrix of electron density, the information about stabilization ($\lambda_2 < 0$) or destabilization ($\lambda_2 > 0$) of the identified non-covalent interaction can be obtained. Generally, the stabilizing interaction (e.g., hydrogen bond) is indicated by the spike in the low-gradient, low-density, and negative λ_2. When a spike shows a positive λ_2, the interaction is repulsive and thus is not present.

***In Vitro* Evaluation.** *Radioligand Binding Assays.* All experiments with using HEK293 cells stably expressing human 5-HT$_{1A}$, 5-HT$_6$, 5-HT$_{7b}$, and D$_{2L}$ receptors and CHO-K1 cells with a plasmid containing the human 5-HT$_{2A}$ receptor coding sequence (PerkinElmer) were conducted according to the procedures described previously elsewhere.[36,37,62] In brief, cells were cultured in 150 cm^2 flasks for membrane preparation. After reaching 90% confluence, they were washed with phosphate-buffered saline (PBS) and centrifuged (200*g*) in PBS supplemented with 0.1 mM EDTA and 1 mM dithiothreitol. Then, cell pellets were homogenized using an Ultra Turrax tissue homogenizer and centrifuged twice (35,000 *g* for 15 min at 4 °C), with incubation for 15 min at 37 °C between the centrifugations.

All assays were carried out in 96-well plates (total volume of 200 μL) in dedicated buffers.

The reaction was performed for 1 h at 37 °C, except 5-HT$_{1A}$R and 5-HT$_{2A}$R, incubated at room temperature (rt) and 27 °C, respectively. Rapid filtration through UniFilter-96 (PerkinElmer) plates with cell harvester was used to terminate the equilibration process. A MicroBeta (PerkinElmer) plate reader was then used to quantify the radioactivity retained on the filters (PerkinElmer, USA). For displacement studies, the following are assay samples contained as radioligands (PerkinElmer, USA): 2.5 nM [^{3}H]-8-OH-DPAT (PerkinElmer, #NET929001MC) for 5-HT$_{1A}$R; 1 nM [^{3}H]-ketanserin (PerkinElmer, #NET791250UC) for 5-HT$_{2A}$R; 2 nM [^{3}H]-LSD (PerkinElmer, #NET638250UC) for 5-HT$_6$R; and 0.8 nM [^{3}H]-5-CT (PerkinElmer, #NET1188U100UC) for 5-HT$_7$R or 2.5 nM [^{3}H]-raclopride (PerkinElmer, #NET975001MC) for D$_{2L}$R. For the determination of non-specific binding, 10 μM 5-HT for 5-HT$_{1A}$R and 5-HT$_7$R, 20 μM mianserin for 5-HT$_{2A}$R, 10 μM methiothepine for 5-HT$_6$R, and 10 μM haloperidol for D$_{2L}$ were used. Each compound was tested in triplicate at seven concentrations in the range from 10^{-10} to 10^{-4} M. The inhibition constants (K_i) were calculated from the Cheng–Prusoff equation.[63]

Moreover, compound **7e** was evaluated for the binding for α_1 and β_1-adrenergic receptors, *h*ERG potassium channels, muscarinic M$_1$ receptors, and histaminic H$_1$ receptor at Eurofins. The results were reported as the % inhibition of the control binding following the experimental protocols at https://www.eurofins.com/.

Radioligand Binding Experiment on Astrocytes. The mouse astrocyte C8-D1A line was purchased from the American Type Culture Collection and cultured as the manufacturer's recommendation. The membranes were prepared in a buffer containing 50 mM Tris-HCl, 0.5 mM EDTA, and 4 mM $MgCl_2$ in the same manner as described in the Radioligand Binding Assays section.

For binding studies, the assay samples contained as radioligand 2 nM [^{3}H]-LSD (PerkinElmer, USA). The level of specific binding for 5-HT$_6$R was obtained by measuring the difference between the total signal from the vehicle and non-specific controls. Non-specific binding was defined with 10 μM compound **7e**, SB258585, intepirdine, and serotonin.

Determination of cAMP Production in 1321N1 Cells. The potency of compounds to the inhibition of cAMP production induced by 5-CT (EC$_{90}$ = 1000 nM), a 5-HT$_6$R agonist, was examined. Compounds **7b**, **7e**, **7f**, **7h**, and **7l** were tested in triplicate at eight concentrations in the range from 10^{-11} to 10^{-4} M. The cAMP level was measured using frozen recombinant 1321N1 cells expressing the Human Serotonin 5-HT$_6$R (PerkinElmer, #ES-316-CF). According to the manufacturer's recommendations, cAMP was measured using the LANCE ULTRA cAMP detection kit (PerkinElmer, #TRF0263). In brief, cells (5 μL) were incubated with a mixture of compounds (5 μL) for 30 min at room temperature in an OptiPlate-384 (PerkinElmer, #6007299) microtiter plate. Next, the reaction was stopped by adding 10 μL of detection solution (Eu-labeled cAMP tracer and ULight antibodies). The plate was incubated at RT for 1 h before measuring the signal with a Tecan multimode plate reader (Infinite M1000 Pro). K_b constants were calculated from the Cheng–Prusoff equation[63] adapted to functional assays.

Determination of cAMP Production in NG108-15 Cells. The cell culture medium for NG108-15 cells was Dulbecco's modified Eagle's medium (DMEM) supplemented with 10% dialyzed fetal calf serum, 2% HAT (hypoxanthine/aminopterin/thymidine) (Life Technologies), and a penicillin–streptomycin solution. To perform cAMP measurement, we used the bioluminescence resonance energy transfer (BRET) sensor for cAMP, CAMYEL (cAMP sensor using YFP-Epac-RLuc).[64] NG108-15 cells were transiently co-transfected in suspension with plasmids encoding the 5-HT$_6$R (0.5 μg DNA/million cells) and CAMYEL constructs (1 μg DNA/million cells), using Lipofectamine 2000, according to the manufacturer's protocol. Cells were distributed in white 96-well plates (Greiner), at a density of 50,000 cells per well. Twenty-four hours after transfection, cells were washed with PBS containing calcium and magnesium. To test the antagonist properties of compounds **7b**, **7e**, **7f**, **7h**, and **7l**, cells were then treated with 10 nM WAY181187 alone or with tested compounds at the concentrations ranging from 0.1 nM to 10 μM. To test the inverse agonist properties of selected compounds and intepirdine, cells were treated with vehicle or with the tested compound at a concentration ranging from 0.1 nM to 10 μM. Coelenterazine H (Molecular Probes) was added at a final concentration of 5 μM. BRET was measured 5 min after addition of coelenterazine H, using a Mithras LB 940 plate reader (Berthold Technologies). The expression of 5-HT$_6$R in NG108-15 cells induced constitutive cAMP production, which is measured as a strong decrease in CAMYEL BRET signal in cells expressing both the CAMYEL and 5-HT$_6$R, when compared with cells transfected with CAMYEL alone. This decrease in CAMYEL BRET signal was thus used as an index of 5-HT$_6$R constitutive activity at Gs signaling.

*Determination of 5-HT$_{1A}$R Agonist/Antagonist Properties for Compound **7e**.* Human 5-HT$_{1A}$R cell line (HEK293) was cultured at 37 °C (5% CO_2) in growth medium (DMEM supplemented with 10% fetal bovine serum and 500 μg/mL geneticin). For functional experiments, cells were grown to 90% confluence. The obtained cell pellet was suspended in a stimulation buffer (1 × HBSS, 5 mM HEPES, 0.5 mM IBMX, and 0.1% BSA). Identification of the mode of action (ago, antago) of compound **7e** was evaluated using a LANCE Ultra cAMP detection kit (PerkinElmer). 5-HT$_{1A}$Rs in HEK293 cells are coupled to the Gαi subtype and decrease cAMP production. Cells

https://dx.doi.org/10.1021/acs.jmedchem.0c02009
J. Med. Chem. 2021, 64, 1180–1196

were stimulated with 1 μM forskolin (EC_{90}). Each compound was examined in the range of 10^{-11} to 10^{-4} M in triplicate. For quantification of cAMP levels, cells (5 μL) were incubated for 30 min at RT with 5 μL of a solution containing the tested ligand and forskolin with or without 1 μM *R*-(+)-8-OH-DPAT (for the test of agonist or antagonist properties, respectively) in an OptiPlate-384 (PerkinElmer, #6007299). The further steps were similar according to a determination of cAMP level in 1321 N1 cells.

Assessment of Preliminary ADME/Tox Properties. In Vitro Metabolic Stability. Metabolic stability assay was executed using an incubation system composed of the tested compound (10 μM), rat liver microsome (microsome from rat male liver, pooled; 0.2 mg/mL; Sigma-Aldrich), and NADPH-regenerating system (NADP+, glucose-6-phosphate and glucose-6-phosphate dehydrogenase in 100 mM potassium buffer, pH 7.4; all from Sigma-Aldrich). The tested 10 μM compound (**7b**, **7e**, **7f**, **7h**, and **7l**) solutions were prepared in methanol. The final concentration of methanol in the incubation mixture was lower than 0.1%. All samples were prepared in duplicate. After pre-incubation of all samples contained the incubation mixture (without NADPH-regenerating system) in thermoblock at 37 °C for 10 min, the reaction was initiated by the addition of the NADPH-regenerating system (in control replaced with potassium buffer). Probes were incubated for 15 and 30 min at 37 °C, then the internal standard (pentoxifylline, 10 μM) was added, and the biotransformation process was stopped by the addition of perchloric acid. Next, samples were centrifuged and supernatants were analyzed by UPLC/MS (Waters Corporation, Milford, MA). The results were evaluated in Graph Pad Prism software using non-linear regression to calculate the half-life time and intrinsic clearance by the equation: Cl_{int} = (volume of incubation [μL]/protein in incubation [mg]) × 0.693/$t_{1/2}$.[65]

Parallel Artificial Membrane Permeability Assay. Parallel artificial membrane permeability assay (PAMPA) was performed using a Corning Gentest Pre-coated PAMPA Plate System, according to the manufacturer's instructions. Compound **7e** (100 μM) was incubated on plates in PBS at pH 7.4 for 5 h at room temperature. The UPLC/MS method was used to determine concentrations of **7e** in donor and acceptor solutions. Pentoxifylline was used as an internal standard. Membrane permeability, expressed as log Pe, was estimated as follows:

$$\log Pe = \log\left(\frac{-\ln\left[1 - C_A/\frac{C_D \times V_D + C_A \times V_A}{V_D + V_A}\right]}{A \times \left(\frac{1}{V_D} + \frac{1}{V_A}\right) \times t}\right)$$

where C_D and C_A are the final concentrations after incubation; the membrane surface area (A) equals 0.3 cm^2; the incubation time (t) is 18,000 s, and the volume of the donor (V_D) and the acceptor (V_A) solutions are 0.3 and 0.2 mL, respectively.

Assessment of Hepatotoxicity and Neurotoxicity. Cell Culture. Human hepatocellular carcinoma cells (HepG2) and human neuroblastoma cells (SH-SY5Y) were cultured using a standard protocol derived from the ATCC in Eagle's minimum essential medium (EMEM) in flasks with an area of 25 cm^2 incubated at 37 °C, in a humidified atmosphere with 5% CO_2. The medium was supplemented with 10% of fetal bovine serum (FBS, Life Technologies) with the addition of 100 IU/mL penicillin (Sigma-Aldrich) and 100 μg/mL streptomycin (Sigma-Aldrich). Before experiments, cells were grown for 24 h in the incubator (37 °C, 5% CO_2) on 96-well culture plates (Falcon) at a density of 2×10^4 cells per well in fresh medium. Tested compounds **7e** and PZ-1444 were added at a concentration ranging from 0.1 to 50 μM and incubated for 24 h. DOX was used as a reference standard in a concentration ranging from 0.1 to 20 μM.

MTT assay. Cell viability was assessed using the MTT assay.[66] Cells were seeded in 96-well plates and exposed to each tested compound for 24 h. Next, 10 μL of MTT reagent (Sigma-Aldrich) was added to each well, and after 4 h of incubation (37 °C, 5% CO_2), the medium was aspirated and 100 μL of DMSO was added to each well. Optical density (OD) at 570 nm was determined on a plate reader (Spectra Max iD3, Molecular Devices). Each individual experiment was repeated at least three times.

Evaluation of the Effects of the 5-HT_6R Ligands upon Neurite Growth of NG108-15 Cells. NG108-15 cells were transfected in suspension with plasmids encoding either cytosolic GFP or a GFP-tagged 5-HT_6 receptor using Lipofectamine 2000 (Life technologies). Cells were then plated on glass coverslips. Six hours after transfection, cells were treated with either DMSO (control conditions), compound **7e**, or intepirdine (1 μM). After 24 h of treatment, cells were fixed for 10 min in 4% paraformaldehyde (PFA) supplemented with 4% sucrose. Cells were then incubated in PBS containing 0.1 M glycine for 15 min to quench PFA fluorescence and washed with PBS and then with water. Coverslips were then mounted using a Prolong Gold antifade reagent (Thermo Fisher Scientific). Cells were imaged using an AxioImagerZ1 epifluorescence microscope (Zeiss) using a 20X objective. Neurite length was assessed using the Neuron J plugin of the ImageJ software (NIH).

Assessment of Glioprotective Properties. Astrocytes (C8-D1A cells) were cultured using a standard procedure in a 25 cm^2 flask at 37 °C, in a humidified atmosphere with 5% CO_2 with DMEM (supplemented with 10% FBS). Cells were harvested (in 80−90% confluence) and seeded in 96-well plates at a density of 1×10^4 cells per well. Next, they were pre-incubated with tested compounds for 5 h, then the cytotoxic agent DOX (10 μM) was added to the medium, and the experimental mixture was incubated for an additional 3 h period. Alternatively, analyzed compounds were pre-incubated for 12 h, and then 6-OHDA (25 μM) was added for an additional 24 h. The ability of compounds to prevent DOX/6-OHDA-induced cytotoxicity was assessed by using the MTT (see the MTT Assay section) and LDH assays.

LDH Assay. Cells were cultured in standard condition and seeded at a density of 12×10^4 cells/per well in 96-well plates for 24 h. Then, cells were pre-incubated with tested compounds for 5 h. Subsequently, DOX (10 μM) was added to the medium, and cells were incubated for an additional 3 h. Alternatively, tested compounds were pre-incubated for 12 h, and after addition of 6-OHDA, (25 μM) cells were incubated for an additional 24 h. After incubation, plates were centrifuged (200*g*, 2 min) and 50 μL of the supernatant was transferred into the corresponding 96-well plate. Then, each well was filled with the LDH-reaction mixture (50 μL) prepared according to the manufacturer's instructions (Invitrogen). Next, stop solution was added and absorbance was measured at 490 nm (A490) using a plate reader (Spectra Max iD3, Molecular Devices). Cytotoxicity percentage was calculated according to the formula: cytotoxicity (%) = [(compound LDH activity − spontaneous LDH activity)/(maximum LDH activity − spontaneous LDH activity)] × 100. Three independent experiments were performed for each condition.

***In Vivo* Pharmacological Evaluation.** The experiment was done in line with the NIH Guide for the Care and Use of Laboratory Animals and has been approved by the Animal Research Ethics Committee at the Maj Institute of Pharmacology. We used male Sprague-Dawley rats (Charles River, Germany) weighing ∼250 g on arrival. Animals were kept under standard laboratory conditions in a colony with A/C room temperature (21 ± 2 °C), humidity of 40−50%, light for 12 h (on: at 6 AM), and unrestricted access to food and tap water. The rats were allowed to acclimate for at least 7 days before starting the experimental procedure. Within this week, the animals were touched and handled at least three times. Behavioral tests were carried out in the light phase of the light/dark cycle. At least 1 h before the start of the experiment, the rats were transferred to the experimental room for acclimatization.[67,68] The rats were tested in a dimly lit (25 lx) opaque gray plastic "open-field" arena (66 × 56 × 30 cm); its floor was cleaned and dried after each measurement.

Drug Treatment. Scopolamine (SCOP, purchased from Sigma-Aldrich, Germany) and compound **7e** were solubilized in distilled water and administered at a dose of 1.25 mg/kg (*i.p.*) and 1−3 mg/kg (*p.o.*) 30 and 120 min before familiarization phase (T1), respectively.

Experimental Procedure. One day before the test, the animals were habituated for 5 min to the empty arena. Testing consisted of two trials lasting for 3 min and separated by 60 min intertrial interval

https://dx.doi.org/10.1021/acs.jmedchem.0c02009
J. Med. Chem. 2021, 64, 1180−1196

(ITI).[67,68] During the familiarization trial (T1), two identical objects (A1 and A2) were presented in opposite corners, ~10 cm from the walls of the arena. The objects used were a 250 mL glass beaker (diameter of 8 cm, height of 14 cm) filled with gravel (350 g) and a plastic 250 mL bottle (6 × 6 × 13 cm) filled with sand (450 g). After T1, animals were returned to their home cages. In the recognition trial (T2), one of the objects was replaced with a novel one (A = familiar and B = novel). The sequence of presentations and the location of the objects were randomly assigned to each rat. The animals were considered to explore the objects by looking, licking, sniffing, or touching them. Passive behaviors like leaning against, standing, or sitting on the object were not recorded. Object exploration times were measured using the Any-maze tracking system (Stoelting Co., Illinois, USA). Any rat spending less than 5 s exploring the two objects at T1 or T2 was eliminated from the calculations. Based on the exploration time (E) of two objects, a discrimination index was calculated in accordance with the formula: DI = (EB − EA)/(EA + EB), where EA is defined as the time spent exploring the familiar object and EB is the time spent exploring the novel object.

■ ASSOCIATED CONTENT

Supporting Information

The Supporting Information is available free of charge at https://pubs.acs.org/doi/10.1021/acs.jmedchem.0c02009.

Characterization data for all intermediates; UPLC and HRMS spectra of final compounds; ^{1}H NMR and ^{13}C NMR spectra of intermediates and final compounds; physicochemical properties, CNS MPO and LLE values, quantum calculations of pK_a values, *in silico* metabolic stability assessment, additional molecular dynamics simulation, and radioligand binding results on astrocytes (PDF)

Homology model coordinate file (PDB ID: 4LDE) (PDB)

PDB coordinate file of the 5-HT$_6$R complex with **7e** (PDB_PZ-1727) (PDB)

PDB coordinate file of the 5-HT$_6$R complex with PZ-1444 (PDB_PZ-1444) (PDB)

PDB coordinate file of the 5-HT$_6$R complex with SAM-760 (PDB_SAM-760) (PDB)

Compound characterization checklist (XLS)

SMILE strings of all shown molecules and corresponding biological activity (CSV)

■ AUTHOR INFORMATION

Corresponding Authors

Miroslav Soural − *Faculty of Science, Department of Organic Chemistry, Palacký University, Olomouc 771 46, Czech Republic; Institute of Molecular and Translational Medicine, Faculty of Medicine and Dentistry, Palacký University, Olomouc 779 00, Czech Republic;* orcid.org/0000-0001-7288-8617; Email: miroslav.soural@upol.cz

Paweł Zajdel − *Faculty of Pharmacy, Department of Organic Chemistry, Jagiellonian University Medical College, Kraków 30-688, Poland;* orcid.org/0000-0002-6192-8721; Email: pawel.zajdel@uj.edu.pl

Authors

David Vanda − *Faculty of Science, Department of Organic Chemistry, Palacký University, Olomouc 771 46, Czech Republic;* orcid.org/0000-0002-4360-677X

Vittorio Canale − *Faculty of Pharmacy, Jagiellonian University Medical College, Kraków 30-688, Poland;* orcid.org/0000-0001-7940-9500

Severine Chaumont-Dubel − *Institut de Génomique Fonctionnelle, Univ. Montpellier, INSERM, CNRS, Montpellier 34-094, France;* orcid.org/0000-0001-6860-6891

Rafał Kurczab − *Maj Institute of Pharmacology, Polish Academy of Sciences, Kraków 31-343, Poland;* orcid.org/0000-0002-9555-3905

Grzegorz Satała − *Maj Institute of Pharmacology, Polish Academy of Sciences, Kraków 31-343, Poland*

Paulina Koczurkiewicz-Adamczyk − *Faculty of Pharmacy, Jagiellonian University Medical College, Kraków 30-688, Poland;* orcid.org/0000-0003-2939-224X

Martyna Krawczyk − *Maj Institute of Pharmacology, Polish Academy of Sciences, Kraków 31-343, Poland*

Wojciech Pietruś − *Maj Institute of Pharmacology, Polish Academy of Sciences, Kraków 31-343, Poland*

Klaudia Blicharz − *Faculty of Pharmacy, Jagiellonian University Medical College, Kraków 30-688, Poland*

Elżbieta Pękala − *Faculty of Pharmacy, Jagiellonian University Medical College, Kraków 30-688, Poland*

Andrzej J. Bojarski − *Maj Institute of Pharmacology, Polish Academy of Sciences, Kraków 31-343, Poland;* orcid.org/0000-0003-1417-6333

Piotr Popik − *Maj Institute of Pharmacology, Polish Academy of Sciences, Kraków 31-343, Poland;* orcid.org/0000-0003-0722-1263

Philippe Marin − *Institut de Génomique Fonctionnelle, Univ. Montpellier, INSERM, CNRS, Montpellier 34-094, France;* orcid.org/0000-0002-5977-7274

Complete contact information is available at: https://pubs.acs.org/10.1021/acs.jmedchem.0c02009

Notes

The authors declare no competing financial interest.

■ ACKNOWLEDGMENTS

This study was supported by the National Science Centre, Poland (grant no. 2016/21/B/NZ7/01742), Ministry of Health of the Czech Republic (17-31834A), University of Montpellier, CNRS, INSERM and Agence Nationale de la Recherche (no. ANR-17-CE16-0013-01 and ANR-17-CE16-0010-01), and the statutory activity of the Maj Institute of Pharmacology, Polish Academy of Sciences.

■ ABBREVIATIONS

5-CT, 5-carboxytriptamine; 6-OHDA, 6-hydroxydopamine; AcOH, acetic acid; ANOVA, analysis of variance; BTPP, (*tert*-butylimino)tris(pyrrolidino)phosphorane; DI, discrimination Index; DIEA, *N,N*-diisopropylethylamine; DOX, doxorubicin; ECL, extracellular loop; EtOH, ethanol; LDH, lactate dehydrogenase; LLE, ligand lipophilicity efficiency; mTOR, mechanistic target of rapamycin; mTORC1, mechanistic target of rapamycin complex 1; MTT, 3-[4,5-dimethylthiazol-2-yl]-2,5-diphenyl tetrazolium bromide; NOR, novel object recognition; PCP, phencyclidine; RDG, reduced density gradient; RLM, rat liver microsome; SCOP, scopolamine; SD, standard deviation; TMs, transmembrane domains

■ REFERENCES

(1) Monsma, F. J.; Shen, Y.; Ward, R. P.; Hamblin, M. W.; Sibley, D. R. Cloning and expression of a novel serotonin receptor with high

affinity for tricyclic psychotropic drugs. *Mol. Pharmacol.* **1993**, *43*, 320−327.
(2) de Bruin, N.; Kruse, C. 5-HT$_6$ Receptor antagonists: potential efficacy for the treatment of cognitive impairment in schizophrenia. *Curr. Pharm. Des.* **2015**, *21*, 3739−3759.
(3) de Jong, I. E. M.; Mørk, A. Antagonism of the 5-HT$_6$ receptor − preclinical rationale for the treatment of Alzheimer's disease. *Neuropharmacology* **2017**, *125*, 50−63.
(4) Khoury, R.; Grysman, N.; Gold, J.; Patel, K.; Grossberg, G. T. The role of 5 HT$_6$-receptor antagonists in Alzheimer's disease: An update. *Expert Opin. Invest. Drugs* **2018**, *27*, 523−533.
(5) Meffre, J.; Chaumont-Dubel, S.; Mannoury la Cour, C.; Loiseau, F.; Watson, D. J. G.; Dekeyne, A.; Séveno, M.; Rivet, J.-M.; Gaven, F.; Déléris, P.; Hervé, D.; Fone, K. C. F.; Bockaert, J.; Millan, M. J.; Marin, P. 5-HT$_6$ Receptor recruitment of mTOR as a mechanism for perturbed cognition in schizophrenia. *EMBO Mol. Med.* **2012**, *4*, 1043−1056.
(6) Duhr, F.; Déléris, P.; Raynaud, F.; Séveno, M.; Morisset-Lopez, S.; Mannoury la Cour, C.; Millan, M. J.; Bockaert, J.; Marin, P.; Chaumont-Dubel, S. Cdk5 induces constitutive activation of 5-HT$_6$ receptors to promote neurite growth. *Nat. Chem. Biol.* **2014**, *10*, 590−597.
(7) Pujol, C. N.; Dupuy, V.; Séveno, M.; Runtz, L.; Bockaert, J.; Marin, P.; Chaumont-Dubel, S. Dynamic interactions of the 5-HT$_6$ receptor with protein partners control dendritic tree morphogenesis. *Sci. Signaling* **2020**, *13*, eaax9520.
(8) Kohen, R.; Fashingbauer, L. A.; Heidmann, D. E. A.; Guthrie, C. R.; Hamblin, M. W. Cloning of the mouse 5-HT$_6$ serotonin receptor and mutagenesis studies of the third cytoplasmic loop. *Brain Res. Mol. Brain Res.* **2001**, *90*, 110−117.
(9) Deraredj Nadim, W.; Chaumont-Dubel, S.; Madouri, F.; Cobret, L.; De Tauzia, M. L.; Zajdel, P.; Bénédetti, H.; Marin, P.; Morisset-Lopez, S. Physical interaction between neurofibromin and serotonin 5-HT$_6$ receptor promotes receptor constitutive activity. *Proc. Natl. Acad. Sci. U. S. A.* **2016**, *113*, 12310−12315.
(10) Nikiforuk, A. The procognitive effects of 5-HT$_6$ receptor ligands in animal models of schizophrenia. *Rev. Neurosci.* **2014**, *25*, 367−382.
(11) Zajdel, P.; Marciniec, K.; Satała, G.; Canale, V.; Kos, T.; Partyka, A.; Jastrzębska-Więsek, M.; Wesołowska, A.; Basięska-Ziobroę, A.; Wójcikowski, J.; Daniel, W. A.; Bojarski, A. J.; Popik, P. N^1-azinylsulfonyl-1*H*-indoles: 5-HT$_6$ receptor antagonists with procognitive and antidepressant-like properties. *ACS Med. Chem. Lett.* **2016**, *7*, 618−622.
(12) Grychowska, K.; Satała, G.; Kos, T.; Partyka, A.; Colacino, E.; Chaumont-Dubel, S.; Bantreil, X.; Wesołowska, A.; Pawłowski, M.; Martinez, J.; Marin, P.; Subra, G.; Bojarski, A. J.; Lamaty, F.; Popik, P.; Zajdel, P. Novel 1*H*-pyrrolo[3,2-*c*]quinoline based 5-HT$_6$ receptor antagonists with potential application for the treatment of cognitive disorders associated with Alzheimer's disease. *ACS Chem. Neurosci.* **2016**, *7*, 972−983.
(13) Ivachtchenko, A. V.; Okun, I.; Aladinskiy, V.; Ivanenkov, Y.; Koryakova, A.; Karapetyan, R.; Mitkin, O.; Salimov, R.; Ivashchenko, A. AVN-492, A novel highly selective 5-HT$_6$R antagonist: preclinical evaluation. *J. Alzheimers Dis.* **2017**, *58*, 1043−1063.
(14) Nirogi, R.; Shinde, A.; Kambhampati, R. S.; Mohammed, A. R.; Saraf, S. K.; Badange, R. K.; Bandyala, T. R.; Bhatta, V.; Bojja, K.; Reballi, V.; Subramanian, R.; Benade, V.; Choudary-Palacharia, R.; Bhyrapuneni, G.; Jayarajan, P.; Goyal, V. Discovery and development of 1-[(2-bromophenyl)sulfonyl]-5-methoxy-3-[(4-methyl-1-piperazinyl)methyl]-1H-indol e dimesylate monohydrate (SUVN-502): a novel, potent, selective and orally active serotonin 6 (5-HT$_6$) receptor antagonist for potential treatment. *J. Med. Chem.* **2017**, *60*, 1843−1859.
(15) Lacroix, L. P.; Dawson, L. A.; Hagan, J. J.; Heidbreder, C. A. 5-HT$_6$ receptor antagonist SB-271046 enhances extracellular levels of monoamines in the rat medial prefrontal cortex. *Synapse* **2004**, *51*, 158−164.
(16) Tassone, A.; Madeo, G.; Schirinzi, T.; Vita, D.; Puglisi, F.; Ponterio, G.; Borsini, F.; Pisani, A.; Bonsi, P. Activation of 5-HT$_6$ receptors iInhibits corticostriatal glutamatergic transmission. *Neuropharmacology* **2011**, *61*, 632−637.
(17) Woods, S.; Clarke, N. N.; Layfield, R.; Fone, K. C. F. 5-HT$_6$ Receptor agonists and antagonists enhance learning and memory in a conditioned emotion response paradigm by modulation of cholinergic and glutamatergic mechanisms. *Br. J. Pharmacol.* **2012**, *167*, 436−449.
(18) Karila, D.; Freret, T.; Bouet, V.; Boulouard, M.; Dallemagne, P.; Rochais, C. Therapeutic potential of 5-HT$_6$ receptor agonists. *J. Med. Chem.* **2015**, *58*, 7901−7912.
(19) Berthoux, C.; Hamieh, A. M.; Rogliardo, A.; Doucet, E. L.; Coudert, C.; Ango, F.; Grychowska, K.; Chaumont-Dubel, S.; Zajdel, P.; Maldonado, R.; Bockaert, J.; Marin, P.; Bécamel, C. Early 5-HT$_6$ receptor blockade prevents symptom onset in a model of adolescent cannabis abuse. *EMBO Mol. Med.* **2020**, *12*, No. e10605.
(20) Teng, L. L.; Lu, G. L.; Chiou, L. C.; Lin, W. S.; Cheng, Y. Y.; Hsueh, T. E.; Huang, Y. C.; Hwang, N. H.; Yeh, J. W.; Liao, R. M.; Fan, S. Z.; Yen, J. H.; Fu, T. F.; Tsai, T. F.; Wu, M. S.; Wang, P. Y. Serotonin receptor HTR$_6$-mediated mTORC1 signaling regulates dietary restriction-induced memory enhancement. *PLoS Biol.* **2019**, *17*, No. e2007097.
(21) Andrews, M.; Tousi, B.; Sabbagh, M. N. 5HT$_6$ Antagonists in the treatment of Alzheimer's dementia: current progress. *Neurol. Ther.* **2018**, *7*, 51−58.
(22) Versijpt, J.; Van Laere, K. J.; Dumont, F.; Decoo, D.; Vandecapelle, M.; Santens, P.; Goethals, I.; Audenaert, K.; Slegers, G.; Dierckx, R. A.; Korf, J. Imaging of the 5-HT$_{2A}$ system: age-, gender-, and Alzheimer's disease-related findings. *Neurobiol. Aging* **2003**, *24*, 553−561.
(23) Vanda, D.; Zajdel, P.; Soural, M. Imidazopyridine-based selective and multifunctional ligands of biological targets associated with psychiatric and neurodegenerative diseases. *Eur. J. Med. Chem.* **2019**, *181*, 111569.
(24) Vanda, D.; Soural, M.; Canale, V.; Chaumont-Dubel, S.; Satala, G.; Kos, T.; Funk, P.; Fülöpova, V.; Lemrova, B.; Koczurkiewicz, P.; Pękala, E.; Bojarski, A. J.; Popik, P.; Marin, P.; Zajdel, P. Novel non-sulfonamide 5-HT$_6$ receptor partial inverse agonist in a group of imidazo[4,5-*b*]pyridines with cognition enhancing properties. *Eur. J. Med. Chem.* **2018**, *144*, 716−729.
(25) Ferrero, H.; Solas, M.; Francis, P. T.; Ramirez, M. J. Serotonin 5-HT$_6$ receptor antagonists in Alzheimer's disease: therapeutic rationale and current development status. *CNS Drugs* **2017**, *31*, 19−32.
(26) Haydar, S. N.; Andrae, P. M.; Yun, H.; Robichaud, A. J. 1-(Arylsulfonyl)-4-(piperazin-1-yl)-*1H*-benzimidazoles as 5-hydroxytryptamine-6 ligands. , WO2010056644A8, Nov 18, 2010, OR2010.
(27) Gerasi, M.; Frakolaki, E.; Papadakis, G.; Chalari, A.; Lougiakis, N.; Marakos, P.; Pouli, N.; Vassilaki, N. Design, synthesis and anti-HBV activity evaluation of new substituted imidazo[4,5-*b*]pyridines. *Bioorg. Chem.* **2020**, *98*, 103580.
(28) Llona-Minguez, S.; Höglund, A.; Jacques, S. A.; Johansson, L.; Calderón-Montaño, J. M.; Claesson, M.; Loseva, O.; Valerie, N. C. K.; Lundbäck, T.; Piedrafita, J.; Maga, G.; Crespan, E.; Meijer, L.; Burgos Morón, E.; Baranczewski, P.; Hagbjörk, A.; Svensson, R.; Wiita, E.; Almlöf, I.; Visnes, T.; Jeppsson, F.; Sigmundsson, K.; Jensen, A. J.; Artursson, P.; Jemth, A.; Stenmark, P.; Warpman Berglund, U.; Scobie, M.; Helleday, T. Discovery of the first potent and selective inhibitors of human DCTP pyrophosphatase 1. *J. Med. Chem.* **2016**, *59*, 1140−1148.
(29) Baxter, N. J.; Rigoreau, L. J. M.; Laws, A. P.; Page, M. I. Reactivity and mechanism in the hydrolysis of *β*-sultams. *J. Am. Chem. Soc.* **2000**, *122*, 3375−3385.
(30) Conticello, R.; Liu, R.; Tehim, A.; Xie, W. Alkyl-substituted 3′-compounds having 5-HT$_6$ receptor affinity. US 20100016297A1, *Mar 4*, 2010, OR2010.
(31) Danca, M. D.; Dunn, R.; Tehim, A.; Xie, W. Pyrrolidine-substituted azaindole compounds having 5-HT$_6$ receptor affinity. US20100022581A1, Jan 7, 2010, OR2010.

https://dx.doi.org/10.1021/acs.jmedchem.0c02009
J. Med. Chem. 2021, 64, 1180−1196

(32) Bernotas, R. C.; Antane, S. A.; Lenicek, S. E.; Haydar, S. N.; Robichaud, A. J.; Harrison, B. L.; Zhang, G. M.; Smith, D.; Coupet, J.; Schechter, L. E. 1-(2-Aminoethyl)-3-(arylsulfonyl)-*1H*-pyrrolopyridines are 5-HT_6 receptor ligands. *Bioorg. Med. Chem. Lett.* **2009**, *19*, 6935−6938.
(33) Leeson, P. D.; Springthorpe, B. The influence of drug-like concepts on decision-making in medicinal chemistry. *Nat. Rev. Drug Discovery* **2007**, 881−890.
(34) Ratcliffe, A. J. Medicinal chemistry strategies to minimize phospholipidosis. *Curr. Med. Chem.* **2009**, *16*, 2816−2823.
(35) González-Vera, J. A.; Medina, R. A.; Martín-Fontecha, M.; Gonzalez, A.; de la Fuente, T.; Vázquez-Villa, H.; García-Cárceles, J.; Botta, J.; McCormick, P. J.; Benhamú, B.; Pardo, L.; López-Rodriguez, M. L. A new serotonin 5-HT_6 receptor antagonist with procognitive activity − importance of a halogen bond interaction to stabilize the binding. *Sci. Rep.* **2017**, *7*, 41293.
(36) Kurczab, R.; Canale, V.; Satała, G.; Zajdel, P.; Bojarski, A. J. Amino acid hot spots of halogen bonding: a combined theoretical and experimental case study of the 5-HT_7 receptor. *J. Med. Chem.* **2018**, *61*, 8717−8733.
(37) Partyka, A.; Kurczab, R.; Canale, V.; Satała, G.; Marciniec, K.; Pasierb, A.; Jastrzębska-Więsek, M.; Pawłowski, M.; Wesołowska, A.; Bojarski, A. J.; Zajdel, P. The impact of the halogen bonding on D_2/5-HT_{1A}/5-HT_7 receptor activity of azinesulfonamides of 4-[(2-ethyl)-piperidinyl-1-yl]phenylpiperazines with antipsychotic and antidepressant properties. *Bioorg. Med. Chem.* **2017**, *25*, 3638−3648.
(38) *Metasite, Molecular Discovery*; program version 6.0.1.,2020.
(39) Grychowska, K.; Chaumont-Dubel, S.; Kurczab, R.; Koczurkiewicz, P.; Deville, C.; Krawczyk, M.; Pietruś, W.; Satała, G.; Buda, S.; Piska, K.; Drop, M.; Bantreil, X.; Lamaty, F.; Pękala, E.; Bojarski, A. J.; Popik, P.; Marin, P.; Zajdel, P. Dual 5-HT_6 and D_3 receptor antagonists in a group of 1*H*-pyrrolo[3,2-*c*]quinolines with neuroprotective and procognitive activity. *ACS Chem. Neurosci.* **2019**, *10*, 3183−3196.
(40) Kurczab, R.; Ali, W.; Łażewska, D.; Kotańska, M.; Jastrzębska-Więsek, M.; Satała, G.; Więcek, M.; Lubelska, A.; Latacz, G.; Partyka, A.; Starek, M.; Dąbrowska, M.; Wesołowska, A.; Jacob, C.; Kieć-Kononowicz, K.; Handzlik, J. Computer-aided studies for novel arylhydantoin 1,3,5-triazine derivatives as 5-HT_6 serotonin receptor ligands with antidepressive-like, anxiolytic and antiobesity action in vivo. *Molecules* **2018**, *23*, 2529.
(41) Grychowska, K.; Kurczab, R.; Śliwa, P.; Satała, G.; Dubiel, K.; Matłoka, M.; Moszczyęski-Pętkowski, R.; Pieczykolan, J.; Bojarski, A. J.; Zajdel, P. Pyrroloquinoline scaffold-based 5-HT_6R ligands: synthesis, quantum chemical and molecular dynamic studies, and influence of nitrogen atom position in the scaffold on affinity. *Bioorg. Med. Chem.* **2018**, *26*, 3588−3595.
(42) Hogendorf, A. S.; Hogendorf, A.; Kurczab, R.; Kalinowska-Tluscik, J.; Popik, P.; Nikiforuk, A.; Krawczyk, M.; Satała, G.; Lenda, T.; Knutelska, J.; Bugno, R.; Staroę, J.; Pietruś, W.; Matłoka, M.; Dubiel, K.; Moszczyęski-Pętkowski, R.; Pieczykolan, J.; Wieczorek, M.; Pilarski, B.; Zajdel, P.; Bojarski, A. J. 2-Aminoimidazole-based antagonists of the 5-HT_6 receptor - a new concept in aminergic GPCR Ligand Design. *Eur. J. Med. Chem.* **2019**, *179*, 1−15.
(43) Staroń, J.; Kurczab, R.; Warszycki, D.; Satała, G.; Krawczyk, M.; Bugno, R.; Lenda, T.; Popik, P.; Hogendorf, A. S.; Hogendorf, A.; Dubiel, K.; Matłoka, M.; Moszczyński-Pętkowski, R.; Pieczykolan, J.; Wieczorek, M.; Zajdel, P.; Bojarski, A. J. Virtual screening-driven discovery of dual 5-HT_6/5-HT_{2A} receptor ligands with pro-cognitive properties. *Eur. J. Med. Chem.* **2020**, *185*, 111857.
(44) Johnson, E. R.; Keinan, S.; Mori-Sánchez, P.; Contreras-García, J.; Cohen, A. J.; Yang, W. Revealing noncovalent interactions. *J. Am. Chem. Soc.* **2010**, *132*, 6498−6506.
(45) Contreras-García, J.; Boto, R. A.; Izquierdo-Ruiz, F.; Reva, I.; Woller, T.; Alonso, M. A benchmark for the Non-Covalent Interaction (NCI) index or... is it really all in the geometry? *Theor. Chem. Acc.* **2016**, *135*, 242.
(46) Allen, N. J.; Lyons, D. A. Glia as architects of central nervous system formation and function. *Science* **2018**, *362*, 181−185.
(47) Qian, Y.; Guan, T.; Tang, X.; Huang, L.; Huang, M.; Li, Y.; Sun, H.; Yu, R.; Zhang, F. Astrocytic glutamate transporter-dependent neuroprotection against glutamate toxicity: an in vitro study of maslinic acid. *Eur. J. Pharmacol.* **2011**, *651*, 59−65.
(48) Liu, B.; Teschemacher, A. G.; Kasparov, S. Astroglia as a cellular target for neuroprotection and treatment of neuro-psychiatric disorders. *Glia* **2017**, *65*, 1205−1226.
(49) Lesiak, A. J.; Brodsky, M.; Cohenca, N.; Croicu, A. G.; Neumaier, J. F. Restoration of physiological expression of 5-HT_6 receptor into the primary cilia of null mutant neurons lengthens both primary cilia and dendrites. *Mol. Pharmacol.* **2018**, *94*, 731−742.
(50) Hirst, W. D.; Price, G. W.; Rattray, M.; Wilkin, G. P. Identification of 5-hydroxytryptamine receptors positively coupled to adenylyl cyclase in rat cultured astrocytes. *Br. J. Pharmacol.* **1997**, *120*, 509−515.
(51) Hirst, W. D.; Cheung, N. Y.; Rattray, M.; Price, G. W.; Wilkin, G. P. Cultured astrocytes express messenger RNA for multiple serotonin receptor subtypes, without functional coupling of 5-HT1 receptor subtypes to adenylyl cyclase. *Brain Res. Mol. Brain Res.* **1998**, *61*, 90−99.
(52) Hirst, W. D.; Minton, J. A. L.; Bromidge, S. M.; Moss, S. F.; Latter, A. J.; Riley, G.; Routledge, C.; Middlemiss, D. N.; Price, G. W. Characterization of [^{125}I]-SB-258585 binding to human recombinant and native 5-HT_6 receptors in rat, pig and human brain tissue. *Br. J. Pharmacol.* **2000**, *130*, 1597−1605.
(53) Upton, N.; Chuang, T. T.; Hunter, A. J.; Virley, D. J. 5-HT_6 receptor antagonists as novel cognitive enhancing agents for Alzheimer's disease. *Neurotherapeutics* **2008**, *5*, 458−469.
(54) Schrodinger *MacroModel*. Schrodinger, LLC: New York, NY, 2019.
(55) Bochevarov, A. D.; Harder, E.; Hughes, T. F.; Greenwood, J. R.; Braden, D. A.; Philipp, D. M.; Rinaldo, D.; Halls, M. D.; Zhang, J.; Friesner, R. A. Jaguar: a high-performance quantum chemistry software program with strengths in life and materials sciences. *Int. J. Quantum Chem.* **2013**, *113*, 2110−2142.
(56) Schrodinger *Jaguar PKa*. Schrodinger, LLC: New York, NY 2019.
(57) Łażewska, D.; Kurczab, R.; Więcek, M.; Kamińska, K.; Satała, G.; Jastrzębska-Więsek, M.; Partyka, A.; Bojarski, A. J.; Wesołowska, A.; Kieć-Kononowicz, K.; Handzlik, J. The computer-aided discovery of novel family of the 5-HT_6 serotonin receptor ligands among derivatives of 4-benzyl-1,3,5-triazine. *Eur. J. Med. Chem.* **2017**, *135*, 117−124.
(58) Schrodinger *LigPrep*; Schrodinger, LLC: New York, NY, 2017.
(59) Schrodinger *Epik*; Schrodinger, LLC, New York, NY, 2017.
(60) Harder, E.; Damm, W.; Maple, J.; Wu, C.; Reboul, M.; Xiang, J. Y.; Wang, L.; Lupyan, D.; Dahlgren, M. K.; Knight, J. L.; Kaus, J. W.; Cerutti, D. S.; Krilov, G.; Jorgensen, W. L.; Abel, R.; Friesner, R. A. OPLS3: A force field providing broad coverage of drug-like small molecules and proteins. *J. Chem. Theory Comput.* **2016**, *12*, 281−296.
(61) Schrodinger *Glide*; Schrodinger, LLC: New York, NY, 2017.
(62) Zajdel, P.; Kos, T.; Marciniec, K.; Satała, G.; Canale, V.; Kamiński, K.; Hołuj, M.; Lenda, T.; Koralewski, R.; Bednarski, M.; Nowiński, L.; Wójcikowski, J.; Daniel, W. A.; Nikiforuk, A.; Nalepa, I.; Chmielarz, P.; Kuśmierczyk, J.; Bojarski, A. J.; Popik, P. Novel multi-target azinesulfonamides of cyclic amine derivatives as potential antipsychotics with pro-social and pro-cognitive effects. *Eur. J. Med. Chem.* **2018**, *145*, 790−804.
(63) Cheng, Y.-C.; Prusoff, W. H. Relationship between the inhibition constant (K_i) and the concentration of inhibitor which causes 50 per Cent Inhibition (I_{50}) of an enzymatic reaction. *Biochem. Pharmacol.* **1973**, *22*, 3099−3108.
(64) Jiang, L. I.; Collins, J.; Davis, R.; Lin, K.-M.; DeCamp, D.; Roach, T.; Hsueh, R.; Rebres, R. A.; Ross, E. M.; Taussig, R.; Fraser, I.; Sternweis, P. C. Use of a CAMP BRET sensor to characterize a novel regulation of cAMP by the sphingosine 1-phosphate/G13 pathway. *J. Biol. Chem.* **2007**, *282*, 10576−10584.

https://dx.doi.org/10.1021/acs.jmedchem.0c02009
J. Med. Chem. 2021, 64, 1180−1196

(65) Singh, J. K.; Solanki, A.; Shirsath, S. V. Comparative in-vitro intrinsic clearance of imipramine in multiple species liver microsomes: human, rat, mouse and dog. *J. Drug Metab. Toxicol.* **2012**, *3*, 126.
(66) Sumantran, V. N. Cellular chemosensitivity assays: an overview. *Methods Mol. Biol.* **2011**, *731*, 219−236.
(67) Ennaceur, A.; Delacour, J. A new one-trial test for neurobiological studies of memory in rats. 1: behavioral data. *Behav. Brain Res.* **1988**, *31*, 47−59.
(68) Popik, P.; Hołuj, M.; Nikiforuk, A.; Kos, T.; Trullas, R.; Skolnick, P. 1-Aminocyclopropanecarboxylic acid (ACPC) produces procognitive but not antipsychotic-like effects in rats. *Psychopharmacology* **2015**, *232*, 1025−1038.

https://dx.doi.org/10.1021/acs.jmedchem.0c02009
J. Med. Chem. 2021, 64, 1180−1196